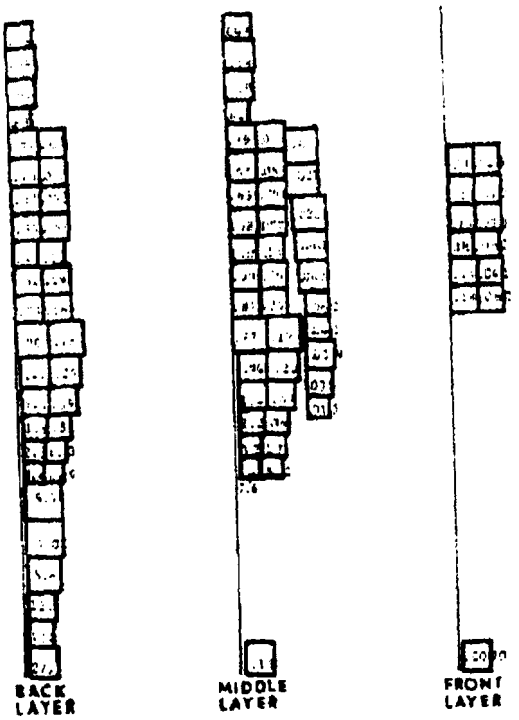

Fig. 5. Local SAR values (W kg⁻¹ per mW cm⁻²) × 100 for inhomogeneous model of man standing on a ground plane at 10 MHz.

cies. Above a frequency of about 200 MHz, part- and whole-body SAR values show little dependence on the presence of a ground plane.

4. REFLECTOR EFFECTS

All calculations of reflector effects have assumed that a man is standing in front of a reflector that is perfectly conducting and infinite in extent. The incident field is vertically polarized with **k** directed from the ventral to the dorsal aspect of the man. One image is required for a flat reflector and three are needed for a 90° corner reflector.

The enhancement of SAR due to reflector effects is approximately the same as the ratio of effective area of a half-wave dipole with a reflector to that of an isolated dipole in free space [*Gandhi et al.*, 1977b]. Antenna theory has been used to perform numerical calculations made for the model of man. Standard procedures have been used for computation of the required values of mutual impedance of dipoles [*Baker and LaGrone*, 1962].

Figures 9-12 show the enhancement of energy absorption as calculated for the model of man with reflector effects and the corresponding gain-enhancement factors calculated for thin dipoles from antenna theory. Values of enhancement for the whole-body average SAR have been used in preparing Figures 9-12, but the curves for part-body energy absorption are nearly identical, which indicates that the distribution of energy through the model is almost independent of the presence of a reflector. Experimental values in Figures 9-12 are for models of man and were reported earlier [*Gandhi et al.*, 1977b].

Figures 9 and 10 show the variation of enhancement of energy absorption as a function of spacing from a reflector at the free-space resonant frequency of 77 MHz. In Figure 9 the numerical values for the model of man are markedly below the curve for thin dipoles at small values of separa-

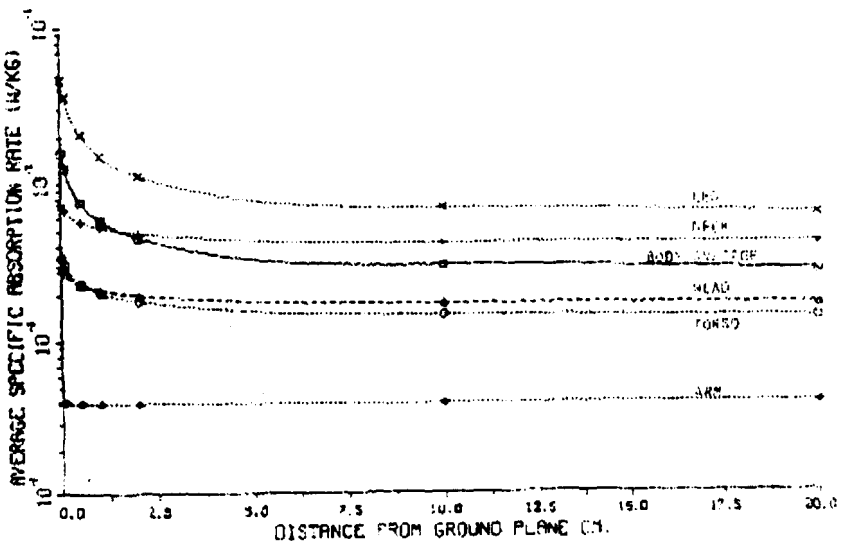

Fig. 6. Whole-body SARs in man for different spacings from the ground at 10 MHz. $E \parallel \hat{L}$, k ventral to dorsal, incident power density of 1 mW cm⁻².

tion. Anten
the spacing
dipole, but
approximat
Figures 1
energy abs
ratios of
calculations
1.75 meter
Figures 11
over a wide
man have
which is no
Figures 11
the SAR at

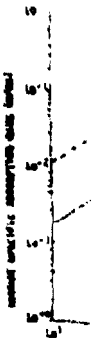

Fig. 8. Whol
ventral

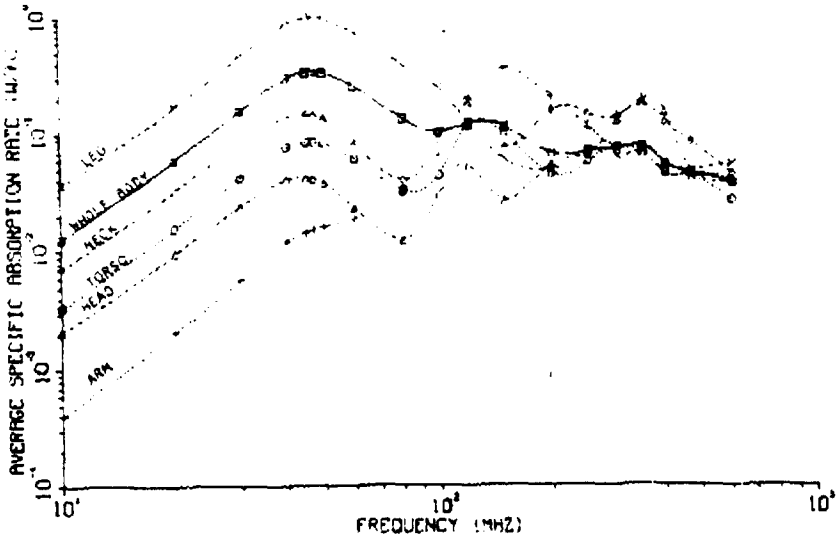

Fig. 7. Part-body SARs for a homogeneous model of man on a ground plane; $E \parallel \hat{L}$, k ventral to dorsal, incident power density of 1 mW cm^{-2}.

tion. Antenna theory requires that the gain be small when the spacing is not much greater than the thickness of the dipole, but such variation is missed in the thin dipole approximation.

Figures 11 and 12 show the variation of enhancement of energy absorption as a function of frequency for fixed ratios of spacing to wavelength. The antenna-theory calculations were made for a thin dipole with a length of 1.75 meters, which is identical to the height of the model. Figures 11 and 12 show that the reflector effects are found over a wide range of frequencies. Values for the model of man have a pronounced roll-off at higher frequencies, which is not seen in calculations for the thin dipoles. In Figures 11 and 12 it can be seen that the rate of roll-off of the SAR at high frequencies is consistent with experimental results that are obtained from models of man. Antenna theory requires that the gain decrease at higher frequencies when the effective area of the dipole images is blocked by the physical cross section of the dipole, but such variation is missed in the thin-dipole approximation.

All gain calculations have been based on zero-order antenna theory; that is, they have no correction for non-sinusoidal current distributions. Significant first- and second-order corrections are required when the antennae are not very thin and the half-length is much different from $\lambda/4$ [*King*, 1956]. The sizable lateral extent of the model of man is thought to be responsible for the difference between

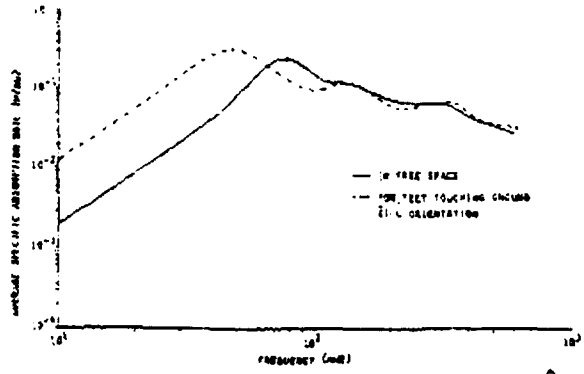

Fig. 8. Whole-body SARs for homogeneous model of man; $E \parallel \hat{L}$, k ventral to dorsal, incident power density of 1 mW cm^{-2}.

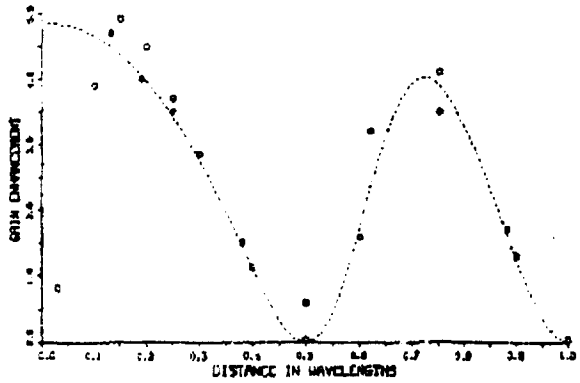

Fig. 9. Variation of gain enhancement with spacing for a half-wave dipole in front of a flat reflector. Squares represent numerical solutions for enhancement of SARs in man at 77 MHz (L/λ = 0.45). Solid circles represent experimental values for anatomically scaled figurines at L/λ = 0.417.

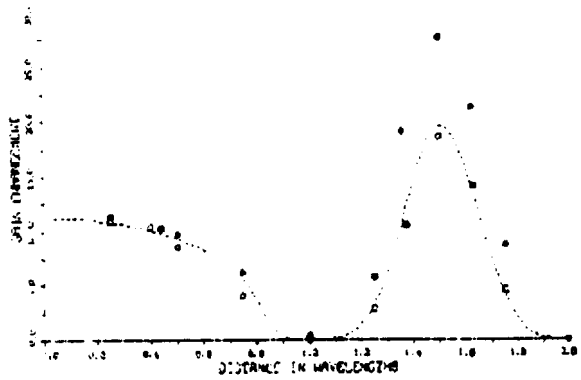

Fig. 10. Variation of gain enhancement with spacing for a half-wave dipole in front of a 90° corner reflector. Squares represent numerical solutions for enhancement of the SAR in man at 77 MHz ($L/\lambda = 0.45$). Solid circles represent experimental values for anatomically scaled figurines at $L/\lambda = 0.417$.

numerical solutions and antenna theory at low frequencies in Figure 12.

The numerical solutions indicate that for frequencies near resonance, the enhancement in SAR due to a reflector is approximately equal to the enhancement in gain of a half-wave dipole with the same reflector configuration. Experimental studies on models of man have also shown that the enhancement of SAR is equal to the enhancement in gain of a dipole, but the gain must be calculated for the finite experimental reflector rather than for an infinite reflector having the same dihedral angle. For certain combinations of length and width of the reflecting sheets, a finite corner reflector may exhibit supergain — a gain significantly greater than that for infinite reflecting planes [*Cottany and Wilson*, 1958; *Schelkunoff and Friis*, 1952].

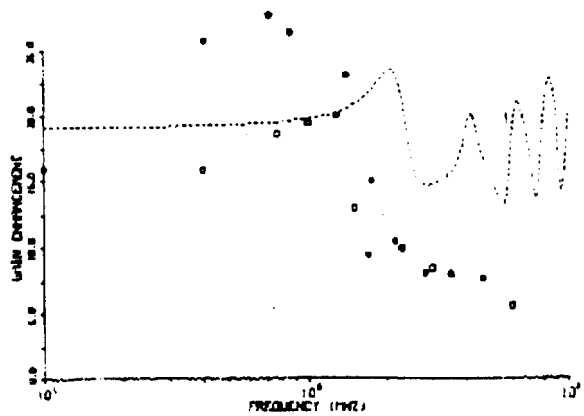

Fig. 11. Variation of gain enhancement with frequency for a 1.75-meter dipole 0.75 λ from a flat reflector. Squares represent numerical solutions for enhancement of SARs in man. Solid circles represent experimental values for anatomically scaled figurines.

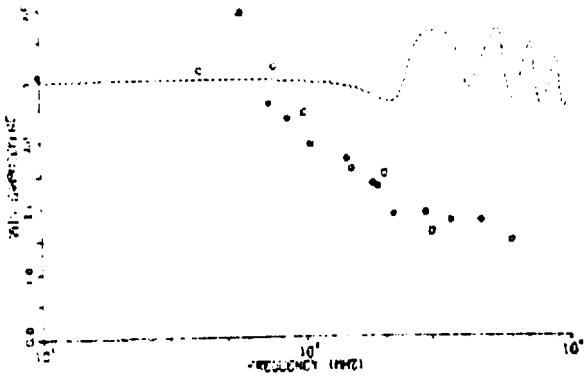

Fig. 12. Variation of gain enhancement with frequency for a 1.75-meter dipole 1.5 λ from a 90° corner reflector. Squares represent numerical solutions for enhancement of SARs in man. Solid circles represent experimental values for anatomically scaled figurines.

Examples of the effect of such supergain combinations are seen in the experimental values in Figures 10-12.

Figures 13 and 14 were copied from an experimental study of finite-size corner reflectors [*Cottany and Wilson*, 1958]. In both figures the angle of the aperture was adjusted for maximum gain at a particular distance of the dipole from the reflector. For reflector lengths greater than about 0.5 λ (Figure 13), the aperture angle is 90° and distance of the dipole from the reflector is 1.5 λ. For reflector lengths greater than 1.0 λ (Figure 14), the aperture angle

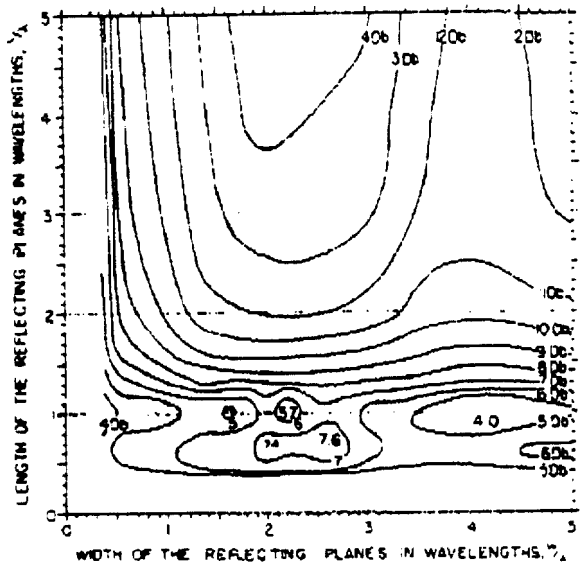

Fig. 13. Contours of constant gain for a corner-reflector antenna with the dipole in third position for various reflector sizes. For lengths greater than ~ 0.5 λ, the aperture angle is 90° and the distance of the dipole from the reflector is 1.5 λ [*Cottany and Wilson*, 1958].

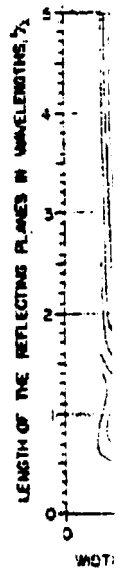

Fig. 14. Cont
with the dipo
lengths great
distance of t

is 65° and d
Note in F
and widths
SAR over t
greater than
combinatior
as much as
12.9 dB (19.
tor of 16 tha
fields in the
tor. As is sho
the reflector
and 12 corre
Supergain
sent for a 6
calculations
reflectors ha
integer. As
limited to su
enhancement
reflectors.

Image the
reflector effi
perfectly con
infinite exten
of finite siz

E 7-2B

EPA-600/8-83-026F
September 1984

Biological Effects of Radiofrequency Radiation

Edited by

Joe A. Elder and Daniel F. Cahill
Health Effects Research Laboratory
Research Triangle Park, North Carolina 27711

Health Effects Research Laboratory
Office of Research and Development
U.S. Environmental Protection Agency
Research Triangle Park, North Carolina 27711

object to intercept or "pull in" considerably more of the energy incident upon it relative to the optical case.

The terms "scattering coefficient" and "absorption coefficient," referring to measures of the efficiency with which an object scatters and absorbs energy, are defined as the ratio of the scattering to optical cross sections and the absorption to optical cross sections, respectively. Of the two basic measures of interaction, the absorption coefficient is considerably more prominent in the interaction of EM waves with biological bodies. Potentially adverse biological effects are related to the energy that the body is absorbing, not to what is scattered. Because absorption rate is related to internal field strength, it is conceivable that a biological effect could be related to the field strength within the tissue. For this reason, most of the remaining material in this section deals only with the absorptive aspect of the interaction phenomenon.

Some measurements have been made of the scattered fields that surround both human subjects and life-size phantom models exposed to incident microwave fields (Reno 1974). Although this work illustrates well the complex scattered fields surrounding the irradiated subject (see Figure 3-4), no attempts have yet been made to relate the field patterns to what the subject is absorbing. Although it is theoretically possible to determine the energy being absorbed and the internal distribution from measurements of the distribution of externally scattered fields, in practice this determination remains a difficult task and has not yet been attempted. Interest in this area is growing, as evidenced by a recent symposium (IEEE 1980) that addressed methods of obtaining high-resolution images of the internal dielectric structure of a biological target. The methods are based on techniques of probing the scattered fields created when the target is irradiated by an RF field. The scope for future work in this area appears large, particularly in diagnostic applications.

3.2.1.1 Factors Affecting the Absorption of RF Energy by an Irradiated Subject

The greater the efficiency of EM energy coupling into a biological subject, the greater the overall whole-body absorption. The factors that influence the degree of absorptive coupling are listed below and will be discussed in turn:

a. Dielectric composition of subject
b. Object size relative to wavelength of incident field
c. Shape or geometry of subject and its orientation with respect to polarization of incident field
d. Complexity of incident radiation

a. *Dielectric composition of subject*—As mentioned previously, absorptive coupling to the irradiated

Figure 3-5 Dielectric data for tissues in RF range 0.01 to 10 GHz. a: permittivity, b: conductivity.

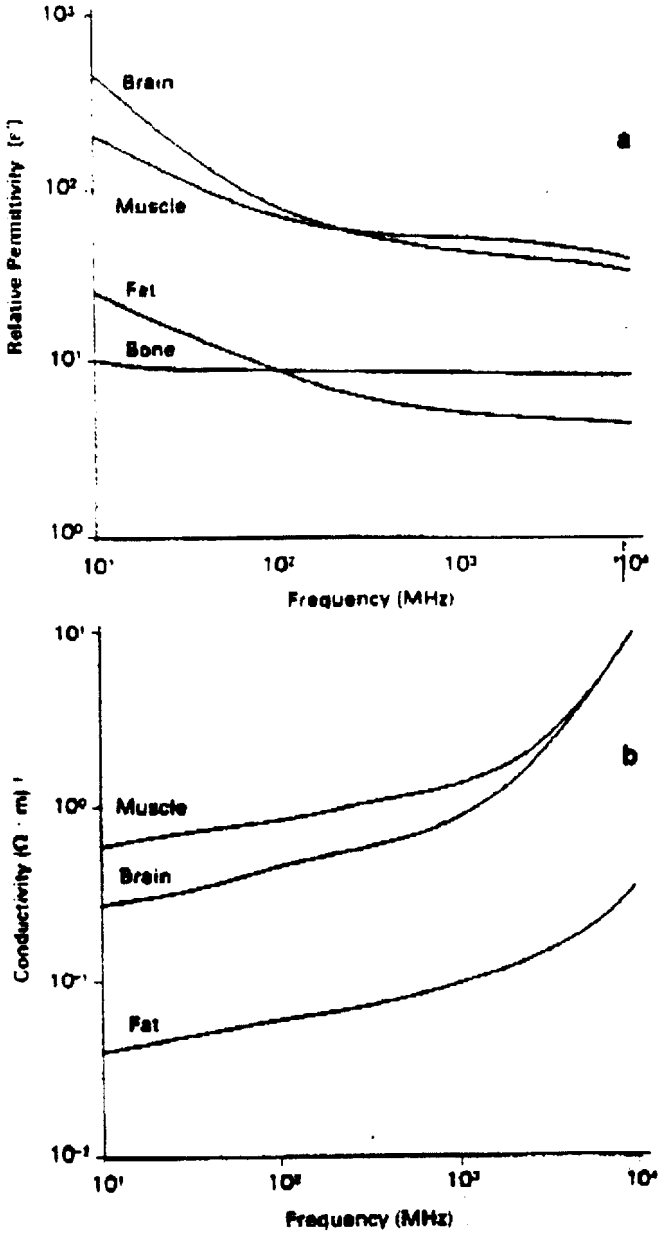

subject can take place only if the subject is composed of dissipative dielectrics of finite conductivity value. The dielectric properties of all biological tissues fall into this category, primarily because their major constituent is water (average of 70 to 80 percent by mass), which contains electrically polarizable or dipolar molecules as well as free ions. The basic mechanism of dissipation of incident RF energy within these tissues is that 1) the free rotations induced in the dipolar water molecules by the externally

Figure 3-6. Illustration of object size vs. wavelength dependence. (Object is composed of tissue-like dispersive dielectric.)

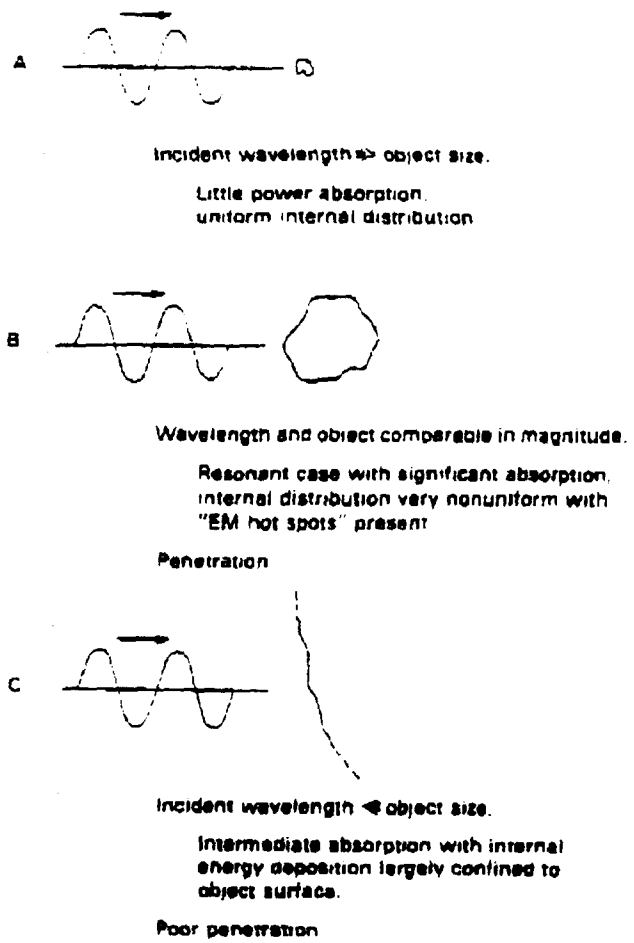

impressed electric field are damped out by collisions with surrounding molecules, and 2) conduction currents are induced within the tissue medium because of the presence of free ions. These phenomena are discussed extensively in Sec. 3.2.4, Mechanisms of RF Interaction with Biological Systems.

Over the past 40 years, many measurements have been made of the dielectric properties of biological tissues. These data have been collected in the *Radiofrequency Radiation Dosimetry Handbook* (Durney *et al.* 1978, Tables 9 and 10), as well as in a more recent paper by Stuchly and Stuchly (1980). The dielectric properties of biological tissues depend to a considerable extent on the water content of the tissue; i.e., tissues of high water content (blood, skin, muscle, brain, etc.) exhibit much higher permittivity (cf. Sec. 3.2.4.1) and conductivity values than do tissues of low water content (fat, bone, etc.). As a result, most incident RF energy tends to pass through the fatty surface tissues of the body and be deposited in the deeper tissues such as muscle and brain. Figure 3-5 illustrates some dielectric data for various types of tissues in the RF range 0.01 to 10 GHz. Note that the dielectric properties of tissue are not constant, but change with frequency. This is an example of what is termed a *dispersive dielectric*. For the case of biological tissues, the dispersive characteristic above 1 GHz is created by the Debye relaxation phenomenon in water molecules (discussed further in Sec. 3.2.4, Mechanisms of RF Interaction with Biological Systems). In part (b) of Figure 3-5, it is apparent that conductivity increases by almost an order of magnitude for all tissues in the frequency range from 1 to 10 GHz. Because of this fundamental dielectric property of tissue, microwaves in the frequency range above about 5 GHz become strongly attenuated in the increasingly lossy tissue medium. Consequently, microwave energy of such frequencies cannot penetrate deeply into body tissues and is deposited near the body surface. As a result of their poor penetration capability, microwaves in the centimetric wavelength region ($\leq$6 cm approximately) are less capable of inflicting potential damage on internal tissue than are those of longer wavelength ($\geq$ 10 cm).

b. *Object size relative to wavelength of incident field*—The second major factor on which energy absorption depends is the size of the irradiated object relative to the wavelength of the incident radiation. Figure 3-6 illustrates that when the wavelength is much greater than the object size (see case A at top of figure), the absorptive coupling is inefficient and little energy is deposited in the object. For this case, called the "subresonant" condition, values of the absorption coefficient lie in the range 0 to 0.5. Case B illustrates the resonant case, which occurs when the wavelength and object dimensions are comparable. For this case, the absorptive efficiency is markedly improved so that significantly more RF energy is coupled into the object and creates much greater deposition. Absorption coefficient values in the range 1.5 to 4 are obtained under resonant conditions. Furthermore, the incident energy penetrates into the object and is deposited internally in a characteristically nonuniform manner, with localized regions of enhanced energy deposition ("EM hot spots") at or near the object's center. These effects are discussed further in later sections of this document. In case C shown at the bottom of Figure 3-6, the wavelength is much shorter than the object size. This represents the quasi-optical case, where the absorptive efficiency is similar to that at optical wavelengths. The absorption coefficient

Figure 3-7. Calculated whole-body average SAR vs. frequency for three polarizations in a prolate spheroidal model of a human; incident power density = 1 mW/cm².

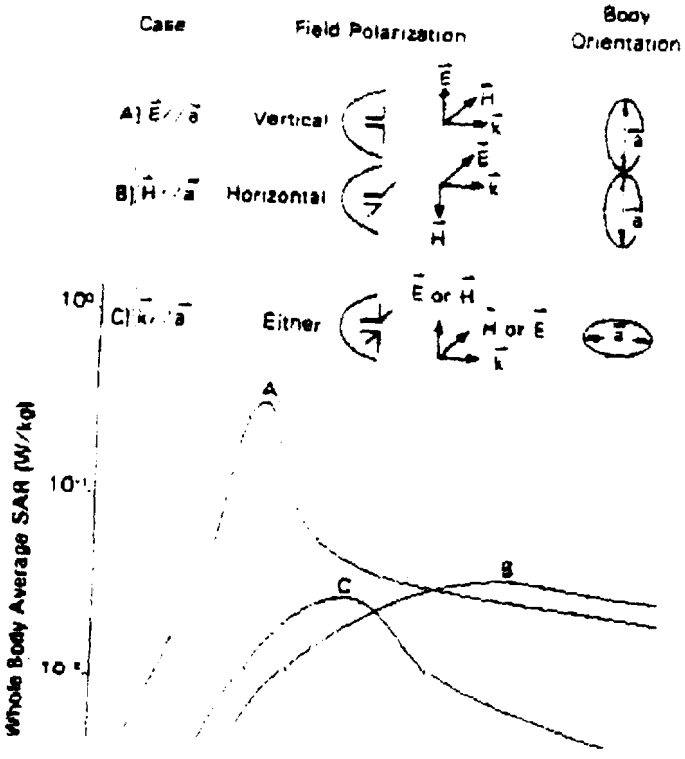

oriented parallel to the major or long axis of the irradiated subject (e.g., a vertically polarized field that is incident on a standing human subject), then the subject absorbs as much as 10 times more energy at resonance than if the electric-field vector is oriented parallel to either of the two minor axes. Figure 3-7 shows absorption characteristics of a prolate spheroid model of an average human. The ordinate represents the whole-body-averaged specific absorption rate (SAR; see Sec 3.2.2, RF Dosimetry Definitions, for discussion of units), and the abscissa represents frequency. From Figure 3-7, it is evident that when the electric-field vector is oriented parallel to the long axis of the prolate spheriod (electric-field polarization case), the absorption curve has a sharp peak at the resonant frequency of ~ 80 MHz. For the other orientations (H- and k-polarization cases), it is apparent that the absorption peak is much broader and occurs at somewhat higher frequencies. Furthermore, the resonant absorption values for the H and k cases are considerably lower than that for the E polarization case. These basic differences in absorption values hold true in both the subresonant and resonant regions, but not in the above-resonant (or quasi optical) region, where absorption in the E- and H- polarization cases is approximately the same.

Figure 3-7. Calculated whole-body average SAR vs. frequency for three polarizations in a prolate spheroidal model of a human; incident power density = 1 mW/cm²

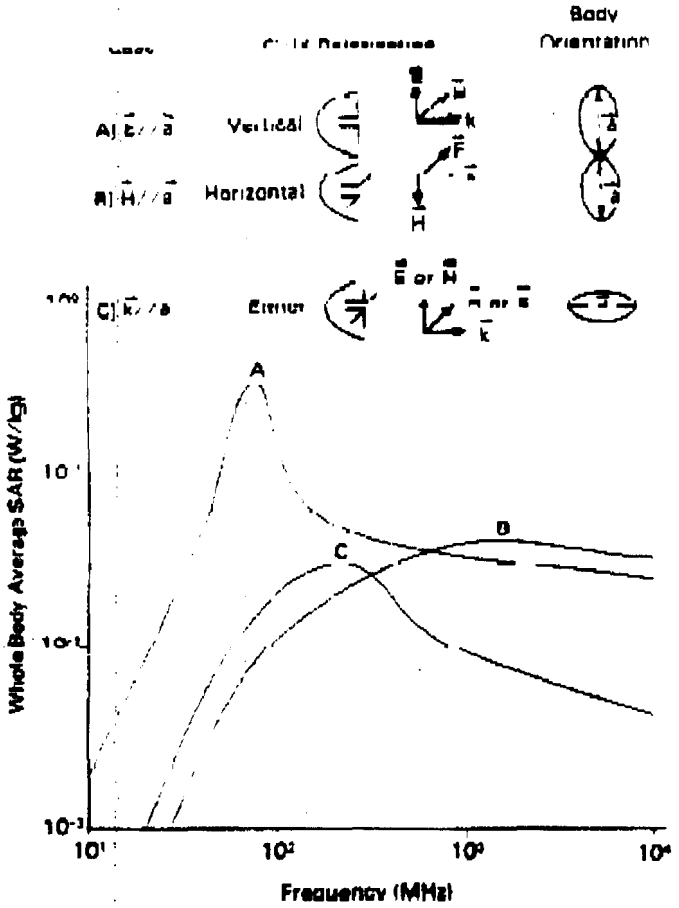

approaches 0.5 under these conditions, which gives intermediate absorption values that fall between those achieved with the conditions of cases A and B. Case C is also characterized by the inability of the incident energy to penetrate much beyond the surface of the object (note the dielectric factors discussed earlier); consequently, the energy coupled into the object under these conditions is confined to the object surface.

c. *Geometry and orientation of subject*—The third factor on which energy absorption depends is the shape of the object and its orientation with respect to the electric-field vector of the incident field. Most biological subjects used in studying the biological effects of RF radiation have a characteristic shape that is significantly elongated along one axis (similarly to humans). Although this observation may appear to be simplistic, it is of considerable significance in the discussion of the interaction of RF waves with such objects. When the electric-field vector of the incident radiation is oriented parallel to the major or long axis of the irradiated subject (e.g., a vertically polarized field that is incident on a standing human subject), then the subject absorbs as much as 10 times more energy at resonance than if the electric-field vector is oriented parallel to either of the two minor axes. Figure 3-7 shows absorption characteristics of a prolate spheroid model of an average human. The ordinate represents the whole-body-averaged specific absorption rate (SAR, see Sec. 3.2.2, RF Dosimetry Definitions, for discussion of units), and the abscissa represents frequency. From Figure 3-7, it is evident that when the electric-field vector is oriented parallel to the long axis of the prolate spheroid (electric-field polarization case), the absorption curve has a sharp peak at the resonant frequency of ~ 80 MHz. For the other orientations (H- and k-polarization cases), it is apparent that the absorption peak is much broader and occurs at somewhat higher frequencies. Furthermore, the resonant absorption values for the H and k cases are considerably lower than that for the E polarization case. These basic differences in absorption values hold true in both the subresonant and resonant regions, but not in the above-resonant (or quasi-optical) region, where absorption in the E and H polarization cases is approximately the same.

d. *Complexity of incident radiation*—The fourth and final factor on which RF-energy absorption depends involves the complexity of the incident radiation. Up to this point, most of the discussions of RF coupling in biological targets have assumed the simplest form of free-field exposure, which involves a unipath plane wave emanating from a distant source and incident on a subject suspended in space. (See Sec. 3.1 for definition of plane wave.) Virtually all the RF-radiation protection guides and standards in use throughout the world are based on this rather idealized assumption. Furthermore, most of the biological experimentation involving free-field exposures in anechoic chambers attempts to simulate this idealized concept. However, real-world, actual exposure conditions are far more complex.

One complicating circumstance arises in the near field. It is readily apparent that the most intense target exposure with the resulting greatest potential for injury would occur close to the RF-radiation source. However, in this near field, the plane-wave assumptions that are true for the far field of the source's radiating antenna no longer hold. As discussed in Sec. 3.1, the near field is characterized by complex EM field properties: the E and H fields are no longer in space quadrature (E and H vectors separated by 90°), and the value of the E/H ratio (termed the wave impedance) differs greatly from the constant value 377 Ω that characterizes the far field.

In the near field, the power density concept is meaningless in its usual sense. For an object placed in the near field of an antenna the interaction is exceedingly complex because every type of antenna possesses near-field characteristics that are unique to that type of radiator. Consequently, [illegible] phenomenon involving near-field exposures must be individually analyzed and characterized. Although it is possible to predict the spatial field distribution in the near field of an antenna, this distribution cannot be used as a basis for predicting the absorptive properties of an object placed in this field because the object will substantially alter that field distribution, as well as alter the radiating charateristics of the antenna itself. When an object is placed in the near field, it interferes with the basic mechanism by which [illegible] RF energy from antennas to far field. An object in the near field tends to load the antenna capacitively, which creates an impedance mismatch if the antenna was originally well matched to free space. As a result, the antenna reflects some of the transmitter energy output back to the source. In general, for an antenna that radiates well in free space, the closer the object is to the antenna, the greater is the mismatch condition, and the poorer is the transfer of radiated energy to the far field. Consequently, it is reasonable to conclude that whole-body-averaged SAR values in the near field do not greatly exceed those existing at the beginning of the far field, although there may be regions within the object of high energy deposition. The limited data available from EM models involving near field exposure (see Sec. 3.2.3) seem to confirm this conclusion.

A concomitant aspect of near-field exposures involves the unwanted exposure to leakage fields emanating from RF devices, such as microwave ovens, RF heat sealers, and diathermy units, which are not intended to radiate energy beyond their immediate surroundings. Such leakage fields are complex, and exposure invariably takes place in the near zone of the leakage source. Nevertheless, the limited data available from near-field exposures of EM models to leakage fields seem to show that whole-body-averaged SAR values are lower than might otherwise be expected because of the leakage-source and near-field interaction effects.

Another aspect of real-world exposures is the so-called multipath problem. People usually stand on the ground and are not suspended in space as in the idealized exposure concept; furthermore, they frequently stand close to buildings or to other reflective surfaces. This situation creates the multipath problem, in which a subject is exposed to scattered as well as to direct energy. Some of the effects are illustrated in Figure 3-8, which shows that there is a considerable enhancement in energy absorption occurring for various multipath conditions. These effects have been illustrated by means of the prolate-spheroid representation of a 70-kg man. To compute the SAR of man for the nonresonant condition, the optical cross-sectional area of the prolate spheroid is first multiplied by the power [illegible] and then the resultant 38 W is divided by 70 kg to give an SAR of 0.54 W/kg. Note that when the model is in contact with a conducting ground plane, there is a doubling of the resonant whole-body energy absorption compared to that of free-space (Case II vs. Case I). Furthermore, if the model is standing at a distance in front of the reflecting plane that corresponds to an eighth of the incident wavelength (Case V, 0.125λ), there is a tenfold increase in absorption relative to that of free space. Such greater increases are recorded when the model is placed at a critical point inside a 90° corner reflector (cases IV and VI). The enhanced absorption is a result of the reflector producing an enhanced field strength at the position of the object and not due to interaction between object and reflector.

In addition to these multipath effects, enhancement of energy absorption can occur because of proximity effects that are created when two or more subjects are simultaneously irradiated. Gandhi *et al.* (1979) have found that when subjects are spaced by a critical separation of 0.65λ, a 50-percent enhancement in absorption can occur. Coupling of RF energy into biological systems is discussed further in the *Radiofrequency Radiation Dosimetry Handbook* (Durney *et al.* 1978, pp. 27-40).

3.2.2 RF Dosimetry Definitions

Dosimetry is the measurement or estimation of RF energy or power deposition in an irradiated subject, including the internal distribution of that deposited energy. In recent years, the terminology describing dosimetric assessment has been evolving. Prior to the mid-seventies most investigators used terminology that appears to have been conveniently borrowed from the ionizing-radiation field and that employed the same cumulative dosage concept (Youmans and Ho 1975; Justesen 1975). Many investigators felt that this terminology was inappropriate for use with nonionizing or RF radiation because energy absorption in this case is not considered a cumulative phenomenon in a way that has been accepted for ionizing radiation (Susskind 1975; Guy 1975). Consequently, a new terminology was proposed that did not use the word "dose." The now widely accepted term "specific absorption rate" (SAR) was first reported in the literature by Johnson (1975); however, the term evolved from joint discussion by members of Scientific Committee 39 of the National Council on Radiation Protection and Measurement (NCRP). (This meeting, chaired by George Wilkening, took place at the Battelle Research Center in Seattle, Washington, on June 23, 1975, with members Frank Barnes, Curtis Johnson, Arthur Guy, Charles

Figure 3-8. Absorption dependence on various ground and multipath factors (Gandhi *et al.* 1977). Note that these data are based on experimental measurements.

Rate of Whole-Body Absorption (WBA) in Watts for a
Prolate Spheroid Model of Man (weight = 70 kg, height = 1.75 m) at 10 mW/cm²

WBA	SAR
Nonresonant conditions	
38 W (no reflectance)	0.54 W/kg
19 W (50% reflectance)	0.27 W/kg
Case I. At resonance for free space.	
151 W	2.16 W/kg, f = 62-68 MHz
Case II. At resonance for conditions of electrical contact with the ground plane.	
2 x 151 = 302 W	4.31 W/kg, f = 31-34 MHz
Case III. At resonance for placement in front of a flat reflector.	
d = 0.125 λ	
4.7 x 151 = 710 W	10.14 W/kg, f = 62-68 MHz

WBA	SAR
Case IV. At resonances for placement in a 90° corner reflector	
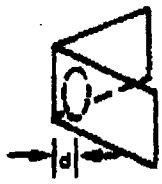	
d = 1.5λ	
27 x 151 = 4077 W	58.24 W/kg, f = 62-68 MHz
Case V. At resonance in electrical contact with ground plane, in front of a flat reflector.	
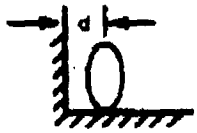	
d = 0.125 λ	
2 x 710 = 1420 W	20.28 W/kg, f = 31-34 MHz
Case VI. At resonance in electrical contact with ground plane in a 90° corner reflector.	
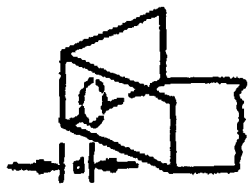	
d = 1.5 λ	
2 x 4077 = 8154 W	116.48 W/kg, f = 31-34 MHz

Susskind, Saul Rosenthal, Karl Illinger, and Ronald Bowman attending. The committee members agreed to publicize the new term as much as possible in their publications to promote wide acceptance. Members Johnson, Susskind, and Guy published comments concerning SAR in 1975.) NCRP (1981) has formally recommended adoption of the term SAR in RF dosimetry. NCRP has also endorsed use of the term "specific absorption" (SA) for the absorbed energy per unit mass (referred to earlier as "dose").

Table 3-2 lists the various RF dosimetric quantities in general use, together with their definitions and units. Although the terms (particularly SA and SAR) for some of these quantities have now gained widespread acceptance, other terms, particularly dealing with the volume-normalized power or energy absorption, have only recently been proposed and have not yet gained wide acceptance.

The mass-normalized and volume-normalized absorption rates are directly related through the localized or whole-body-averaged tissue mass density ρ, that is, absorption-rate density, ARD = ρ(SAR), where ρ is in kilograms per cubic meter. Most biological tissues are composed largely of water, so that it is reasonable to assume a unity tissue density value. In this case, the two quantities are numerically equivalent. This approach has been adopted by many investigators engaged in predictive EM modeling (see Sec. 3.2.3, Analytical and Numerical RF-Electromagnetic Interaction Models), where the model is composed of some homogeneous tissue with average physical and dielectric characteristics that are representative of the various tissues of the body being modeled. For example, all the SAR data given in the familiar *Radiofrequency Radiation Dosimetry Handbook* were derived this way; the assumption of a unity average tissue density is specifically stated (Durney *et al.* 1978).

A subset of two additional values exists for both the mass-normalized and volume-normalized quantities listed in Table 3-2: (a) the whole-body-averaged value, which represents the overall absorption or absorption rate divided by the total mass or volume of the subject; and (b) the localized value, which describes the absorption or absorption rate in an incrementally small mass or volume at some given point within the subject. The localized ARD is mathematically defined by the expression σE^2, where σ is the local tissue conductivity and E represents the root-mean-square value of local internal E-field strength.

So far, there has been no discussion of radiant exposure rate assessment, i.e., measurements of the incident field strength or power density. Some workers unfortunately continue to include such assessment under the general heading of "dosimetry"—incorrectly, because the exposure rate is not an assessment of dose even though the two may be related. The correct terminology for incident power-density assessment is "densitometry," which should not be confounded with dosimetry. Experimental methods used in densitometry are discussed in Sec. 3.3.3, Densitometric Instrumentation. The various experimental techniques that have been developed for whole-body, as well as localized or regional dosimetry, are discussed in detail in Sec. 3.4, Experimental Methods.

3.2.3 Analytical and Numerical RF-Electromagnetic Interaction Models

Much of the discussion concerning the qualitative nature of EM interaction with biological targets contained in Sec. 3.2.1 is based on data derived from mathematical EM models in conjunction with limited experimental confirmation. Predictive physical modeling, used extensively in this research area by many workers during the past 25 years, has contributed significantly toward an improved understanding of the nature of EM field interactions with biological subjects and their absorption characteristics. In these models an object of simplified geometry, composed of dissipative dielectric materials that closely simulate the spatially averaged electrical properties of biological tissues, is irradiated by some form of noncomplex incident field such as a unipath plane wave. Solutions to the problem setup in the model can then be derived by several well-established analytical and numerical techniques. Actual computations are performed on high-speed digital computers, and the outputs represent whole-body-averaged and localized ARD, absorption cross sections, and absorption coefficients.

Besides the improved understanding of the EM interaction process already mentioned, modeling has proved to be important for two further basic reasons. First, mathematical modeling and experimental measurements on scaled-down doll and figurine phantoms have so far provided us with the only practical method of gaining qualitative and quantitative insight into the absorption characteristics of the human body under various conditions of irradiation. Any attempt to make absorption measurements on actual human subjects has so far proven impractical because of technical difficulties, high costs, and ethical considerations. Reasonably accurate quantitative data on human-absorption characteristics are necessary to determine the objective exposure limits for RF radiation. The reasons are discussed below.

The 1974 ANSI-recommended protection guide (ANSI 1974) is based on an allowable exogenous heat load due to RF-energy absorption and conversion that cannot exceed the basic metabolic rate (BMR) in an adult man (~ 70 to 100 W). For a 50th percentile standard-size man weighing 70 kg, this load

Frey, A.H., S.R. Feld, and B. Frey. 1975. Neural Function and Behavior: Defining the Relationship. Ann. N.Y. Acad. Sci., 247:433-439.

Friedman, H.L. 1981. Are Chronic Exposure to Microwaves and Polycythemia Associated? New England J. Med., 304:357-358.

Friedman, H., R.O. Becker, and C.H. Bachman. 1967. Effect of Magnetic Fields on Reaction Time Performance. Nature, 213:949-950.

Froehlich, J.P. 1969. Information Transmittal and Communicating Systems. Holt, Rinehart, and Winston, New York, New York. 274 pp.

Fröhlich, H. 1968. Long Range Coherence and Energy Storage in Biological Systems. Int. J. Quant. Chem., 2:641-649.

Fröhlich, H. 1975. The Extraordinary Dielectric Properties of Biological Materials and the Action of Enzymes. Proc. Natl. Acad. Sci. USA, 72:4211-4215.

Gage, M.I. 1979a. Behavior in Rats after Exposures to Various Power Densities of 2450 MHz Microwaves. Neurobehav. Toxicol., 1:137-143.

Gage, M.I. 1979b. Microwave Irradiation and Ambient Temperature Interact to Alter Rat Behavior Following Overnight Exposure. J. Microwave Power, 14:389-398.

Gage, M.I., E. Berman, and J.B. Kinn. 1979. Videotape Observation of Rats and Mice During an Exposure to 2450 MHz Microwave Radiation. Radio Sci., 14(6S):227-232.

Gale, C.C. 1973. Neuroendocrine Aspects of Thermoregulation. Annu. Rev. Physiol., 35:391-430.

Gale, C.C., M. Mathews, and J. Young. 1970. Behavioral Thermoregulatory Responses to Hypothalamic Cooling and Warming in Baboons. Physiol. Behav., 5:1-6.

Gandhi, O.P. 1980. State of the Knowledge for Electromagnetic Absorbed Dose in Man and Animals. Proc. IEEE, 68(1):24-32.

Gandhi, O.P., E.L. Hunt, and J.A. D'Andrea. 1977. Deposition of Electromagnetic Energy in Animals and in Models of Man with and without Grounding and Reflector Effects. Radio Sci., 12(6S):39-47.

Gandhi, O.P., M.J. Hagmann, and J.A. D'Andrea. 1979. Part-Body and Multi-Body Effects on Absorption of Radio-Frequency Electromagnetic Energy by Animals and by Models of Man. Radio Sci., 14(6S):15-21.

Gavalas, R.J., D.O. Walter, J. Hamer, and W.R. Adey. 1970. Effect of Low-Level, Low-Frequency Electric Fields on EEG and Behavior in Macaca Nemestrina. Brain Res., 18:491-501.

Gavalas-Medici, R., and S.R. Day-Magdaleno. 1976. Extremely Low Frequency, Weak Electric Fields Affect Schedule-Controlled Behavior of Monkeys. Nature, 261:256-258.

Ginoza, W., and R.C. Miller. 1965. Kinetics of X-Ray and Heat Inactivation of ΦX174 RF-DNA. Proc. Natl. Acad. Sci. USA, 54:551-558.

Ginoza, W., C.J. Hoelle, K.B. Veasey, and C. Carmack. 1964. Mechanisms of Inactivation of Single-Stranded Virus Nucleic Acids by Heat. Nature, 203(4945):606-609.

Ginzburg, V.L. 1968. The Problem of High Temperature Superconductivity. Contemp. Phys., 9:355-374.

Goldblith, S.A., and D.I.C. Wang. 1967. Effect of Microwaves on *Escherichia coli* and *Bacillus subtilus*. Appl. Microbiol., 15:1371-1375.

Goldstein, L., and Z. Sisko. 1974. A Quantitative Electroencephalographic Study of the Acute Effects of X-Band Microwaves in Rabbits. In: Biologic Effects and Health Hazards of Microwave Radiation, P. Czerski, K. Ostrowski, M.L. Shore, C. Silverman, M.J. Suess, and B. Waldeskog, eds. Polish Medical Publishers, Warsaw, Poland. pp. 128-133.

Goodman, E.M., B. Greenebaum, and M.T. Marron. 1979. Bioeffects of Extremely Low-Frequency Electromagnetic Fields. Radiat. Res., 78:485-501.

Goodman, R., C.A. L. Bassett, and A.S. Henderson. 1983. Pulsing Electromagnetic Fields Induce Cellular Transcription. Science, 220:1283-1285.

Gordon, C.J. 1982a. Effects of Ambient Temperature and Exposure to 2450-MHz Microwave Radiation on Evaporative Heat Loss in the Mouse. J. Microwave Power, 17:145-150.

Gordon, C.J. 1982b. Open-Loop Gain of Evaporative Heat Loss During Radiant Heat Exposure in the Mouse. Am. J. Physiol. 242:R275-R279.

Gordon, C.J. 1982c. Effect of Heating Rate of Evaporative Heat Loss in the Microwave-Exposed Mouse. J. Appl. Physiol., 53(2):316-323.

Gordon, C.J. 1982d. Rewarming Mice from Hypothermia by Exposure to 2450-MHz Microwave Radiation. Cryobiology, 19:428-434.

Gordon, C.J. 1983a. Behavioral and Autonomic Thermoregulation in Mice Exposed to Microwave Radiation. J. Appl. Physiol., 55:1242-1248.

Gordon, C.J. 1983b. Influence of Heating Rate on Control of Heat Loss from the Tail in Mice. Am. J. Physiol., 244:R778-R784.

Gordon, C.J. 1983c. Effect of 2450 MHz Microwave Exposure on Behavioral Thermoregulation in Mice. J. Thermal Biol., 8:315-319.

Radio Science Vol. 12 (6S) 1977, pg 39-47

E7-2c

Deposition of electromagnetic energy in animals and in models of man with and without grounding and reflector effects

Om P. Gandhi

Departments of Electrical Engineering and Bioengineering, University of Utah, Salt Lake City, Utah 84112

Edward L. Hunt

Department of Microwave Research, Walter Reed Army Institute of Research, Washington, D. C. 20012

John A. D'Andrea

Departments of Electrical Engineering and Bioengineering, University of Utah, Salt Lake City, Utah 84112

Generalized curves are given for rates of whole-body absorption of electromagnetic energy by models of human beings as a function of frequency. Exposures were made in free space, or when the model made electrical contact with the ground. The effects of the presence of reflecting surfaces also were analyzed. Peaks of absorption with and without a ground, are projected, respectively, to be (31 to 34 MHz) and (62 to 68 MHz) × (1.75/height of model in meters). Rates of energy deposition are given for models of man and for animals subjected to radiation at a power density of 10 mW/cm^2 for the various conditions of exposure. At resonance, values of whole-body absorption as high as 4,077 to 8,154 watts for the adult human being are predicted. The times-to-convulsion of ~ 100-g rats at power densities of 3 to 20 mW/cm^2 confirmed predictions of extremely high rates of absorption in the presence of reflecting surfaces.

1. INTRODUCTION

We have previously reported on the observation of a strong resonance in the whole-body absorption of electromagnetic waves by biological bodies [*Gandhi*, 1974, 1975]. For plane-wave irradiation in free space, the highest rate of energy deposition occurs in fields that are polarized along the longest dimension of the body ($\mathbf{E} \| \mathbf{L}$) and for frequencies such that the major length (L) is approximately 0.36 to 0.40 times the free-space wavelength (λ) of radiation. Peaks of whole-body absorption for two other configurations (major length oriented along the direction of wave propagation or along the vector of the magnetic field) were also reported [*Gandhi*, 1974, 1975] for L/λ on the order of $L/4\pi b$ where $2\pi b$ is the weighted averaged circumference of the animals.

A handicap of past measurements has been that commercially available dolls that have been used as molds for models are not properly proportioned. Using carefully sculptured, accurately scaled figurines [*Dreyfuss*, 1967], measurements have now been extended to cover the region $0.2 < L/\lambda < 3.3$. Specific absorption rates (SARs) are given in this paper under three configurations in free space for the frequency range 0.5 to 8.7 times the $\mathbf{E} \| \mathbf{L}$ resonance frequency f_r, which, for man, is 65 × (1.75/length in meters) MHz. From these results, antenna theory is used to develop an empirical equation for the SAR, for the $\mathbf{E} \| \mathbf{L}$ orientation of models, at resonant and supraresonant frequencies. A comparison with the lethality data of *Schrot and Hawkins* [1975] confirms the validity of the equation for rats and mice of differing sizes.

Results are also presented for a simulated human being with its feet in electrical contact with the ground. In such an exposure, a resonant frequency one-half as high with a peak absorption twice that of free-space irradiation is observed.

Energy deposition rates are given for models of man and for animals that were exposed to radiation at power densities of 10 mW/cm^2 under various conditions of exposure.

2. ELECTROMAGNETIC ENERGY ABSORPTION IN MAN IN FREE SPACE

The procedure for obtaining the mass-normalized rate of electromagnetic energy deposition (SAR) through the use of reduced scale models has been detailed in earlier publications [*Gandhi*, 1975; *Gandhi et al.*, 1975]. The SAR in W/kg is calculated from the temperature rise, ΔT, of 7.6, 10.2, 12.7, 15.2, 20.3, 25.4, 33.0, and 40.6 cm high, saline-filled (0.9% NaCl) figurines from the expression (4,180 ΔT × specific heat of the medium in calories/g/°C)/irradiation time in seconds. The SARs so calculated are divided by the model's scaling factor (height of the human/length of the figurine) to obtain the value for a human being. At least three measurements were taken to calculate the averaged SARs that are given in this paper. Unless otherwise stated, the standard deviation of the measurements is less than

± 3%. The values obtained with saline-filled figurines were found to agree with the average of the values for individual parts of the body for tissue-simulating f[illegible], which leads [illegible] to the method of arriving at the whole-body absorption curves for man. A more accurate procedure that is yet to be carried out is calorimetric measurement of whole-body energy deposition in figures that are filled with materials that duplicate the differing conductive and dielectric properties of various tissues.

Curves for whole-body absorption by models of man exposed to radiation in free space are given in Figures 1 and 2. For each of the indicated polarizations the orientation resulting in a maximum rate of energy deposition was used [*Gandhi et al.*, 1975]. These orientations correspond to propagation normal to the sagittal plane – from arm to arm (rather than from front to back) – for E || L orientation; E normal to the sagittal plane (rather than from front to back) for k || L orientation; and E normal to the sagittal plane for H || L orientation.

To date, the experimental data have been obtained to 8.7 times the E || L resonant frequency which lies between 62 to 68 MHz. The quantities plotted in [illegible]

1. The relative absorption coefficient S, which is a measure of the efficiency of energy absorption:

$$S = \frac{\text{Microwave absorption cross section}}{\text{Physical cross section of the body}} = \frac{(\text{Whole body rate of energy absorption in watts}) / (\text{Field intensity in watts/cm}^2)}{\text{Physical cross section of the body in cm}^2}$$

2. The specific absorption rate (SAR) in W/kg.
3. The SAR as compared to basal metabolic rate BMR).

In calculating the SAR-to-BMR ratios for Figures 1 and 2, a basal metabolic rate [*Guyton*, 1966] of 100 kilocalories/hr is assumed which corresponds to 1.66 W/kg for a 70-kg man. A higher metabolic rate (MR) of 1.66 to 1.96 W/kg is assumed to occur during normal activity such as standing while relaxed, dressing and undressing, etc.; use of any number in this range would not appreciably alter the SAR/MR ratios shown in Figures 1 and 2.

For the most highly absorbing E || L orientation, the whole body absorption curve may be discussed in terms of five regions of frequency:

Region 1 – Frequencies well below resonance ($L/\lambda < 0.1$-0.2). An f^2-type dependence derived theoretically and checked experimentally by Durney and coworkers [*Massoudi et al.*, 1975].

Region 2 – Subresonant region ($0.2 < L/\lambda < 0.36$). An $f^{2.75}$ to f^3 dependence of rate of energy deposition has been experimentally observed for this region.

Region 3 – Resonant region ($L/\lambda \simeq 0.36$-0.4). A relative absorption cross section S_{res} on the order of 0.665 $L/2b$ (derivable also from antenna theory [*Gandhi et al.*, 1974]) [illegible] where L is the major length of the body and $2\pi b$ is its weighted cross-sectional circumference. For an adult human [illegible], $L/2b \simeq 6.34$, $S_{res} \simeq 4.21$. This corresponds to SAR/(BMR) (1.75) ≈ [illegible] for an incident power density of 10 mW/cm². For a man of height 1.75 meters, the resonant frequency is on the order of 62 to 68 MHz and at resonance, the SAR is 1.3 times the BMR.

Region 4 – Supraresonant region, i.e., to frequencies on the order of 1.8 S_{res} times the resonant frequency f_r (for human beings this covers the region $f_r < f < 8 f_r$). A whole-body absorption rate reducing as $(f/f_r)^{-1}$ from the resonant value has been observed.

Region 5 – $f \gg f_r$ region. The S parameter should asymptotically approach the "optical" value, which is (1 - power reflection coefficient) or about 0.5.

In comparing the graph of Figure 1 with those of Figure 2 (drawn to the same scale), the following points are noteworthy:

1. For frequencies (4-5) $f_r < f < (8$-$9) f_r$, there is little distinction between averaged rates of energy absorption for the various polarizations. For humans, this corresponds to (frequency in MHz) × (height in [illegible]), [illegible] and 550 MHz.

2. The resonances for k || L and H || L orientations are not very sharp. Indeed, for the H || L orientation, the SAR gradually reaches a peak value and stays at that value at higher frequencies.

3. ENERGY DEPOSITION IN RATS AND MICE FOR FREE-SPACE IRRADIATION

Antenna theory and the observed frequency dependence that is shown in Figure 1 have been used to develop the following empirical equations for rats and mice and for other animals that may be represented by an equivalent prolate spheroid of dimensions L and $2b$ along the major and minor axes, respectively.

$$\text{Resonant frequency } f_r = 11.4/L_{cm} \tag{1}$$

$$S_{res} = 0.665\, L/2b \tag{2}$$

where

$$L/2b = 0.724 \left[\frac{L_{cm}^{\,3}}{\text{mass of the animal in g}} \right]^{1/2} \tag{3}$$

For the supraresonant frequency region $f_r < f < (1.8\, S_{res}) f_r$, and at an incident power density of 10 mW/cm²,

$$SAR \text{ in W/kg} = \frac{59.54}{f_{GHz}} \frac{L_{cm}}{\text{Mass in g}} \tag{4}$$

The equations have been used to generate the generalized curves for rats and mice (Figure 3) under free-space irradiation for the polarization (E || L) that produces

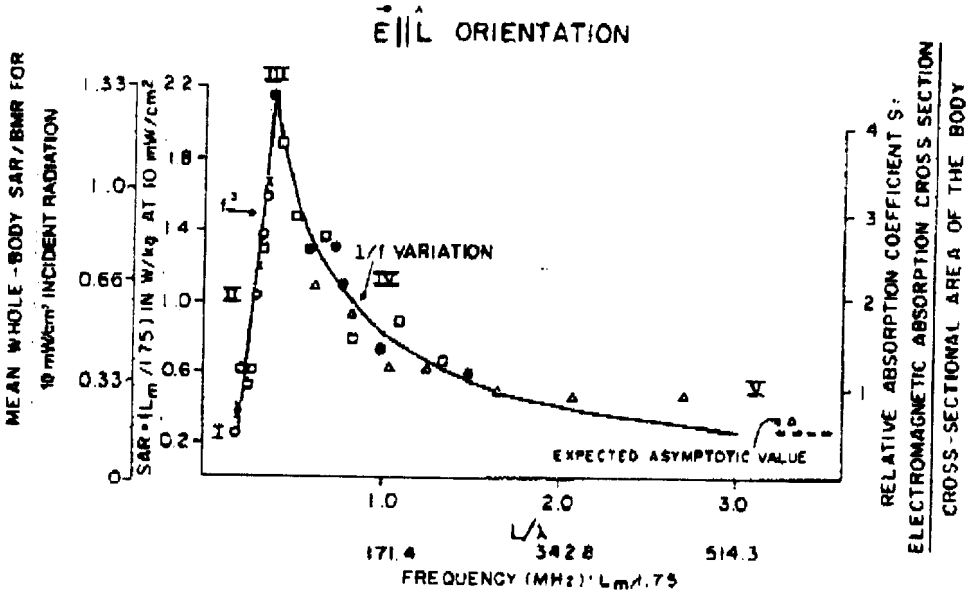

Fig. 1. Whole-body averaged SARs and the relative absorption coefficient, S, of saline-filled models of human beings during microwave irradiation in the free field. The E-field vector is parallel with the long axis of the model. Direction of propagation is normal to sagittal plane. Legend: ○ = prolate spheroids of $(L/2b) = 6$, at 710 MHz; x = human-shaped dolls at 500 MHz (parallel-plate transmission line); ● = human-shaped dolls at 987 and 2450 MHz; □ = accurately proportioned figurines, 7 to 41 cm in length, at 987 MHz; ▲ = the proportioned figurines at 2450 MHz.

the highest SAR. A cross-sectional enhancement factor S_{res} of 2.16 (given from equation (2) [also, *Gandhi et al.*, 1975] for an aspect ratio $L/2b = 3.25$ equivalent prolate spheroid) is assumed in the graphics of Figure 3. Also shown in the figure are the values calculated from the lethality data of *Schrot and Hawkins* [1975]. In calculating the EAR from their data, it is assumed that: (a) an elevation of temperature of 7.4 °C results in a convulsion, and (b) The ΔT occurs in an adiabatic man- [illegible] that there is no other mechanism for gain or loss of heat from the animal's body.

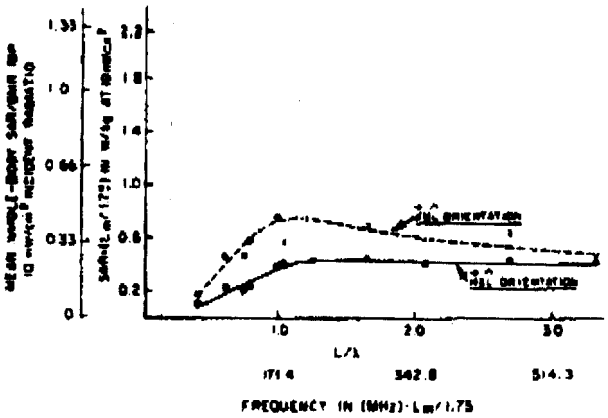

Fig. 2. Whole-body averaged SARs of saline-filled models of human beings during microwave irradiation in the free field. Dashed line: best fit with data-points where propagation vector, k, is parallel with long axis of the model (from head to toe) and E-field vector is normal to sagittal plane. Continuous line: best fit with data points where H-field vector is parallel with long axis of model and E-field vector is normal to sagittal plane. Legend: ● = human-shaped dolls at 987 and 2450 MHz; x = proportioned figurines at 2450 MHz; ○ = human-shaped dolls at 987 and 2450 MHz; ⊕ = proportioned figurines at 2450 MHz.

Because of the high power density (150 mW/cm²) used in the experiments by Schrot and Hawkins, the second assumption may be quite justified. From inspection of Figure 3, it can be seen that there is a good correlation between empirical and experimental values.

4. WHOLE-BODY ABSORPTION BY MAN IN ELECTRICAL CONTACT WITH THE GROUND

Whole-body absorption by a model of a human being with feet in electrical contact with the ground is shown in Figure 4. The results are projected from measurements with 10.2, 12.7, 15.2, and 20.3 cm (height) saline-filled figurines that were exposed to E || L radiation at different frequencies in the monopole-above-ground radiation chamber [*Gandhi*, 1975]. This chamber, which uses a radiator that is a quarter-wave above ground, provides in conjunction with figurines a proper simulation of grounding effects on energy absorption. Comparing the

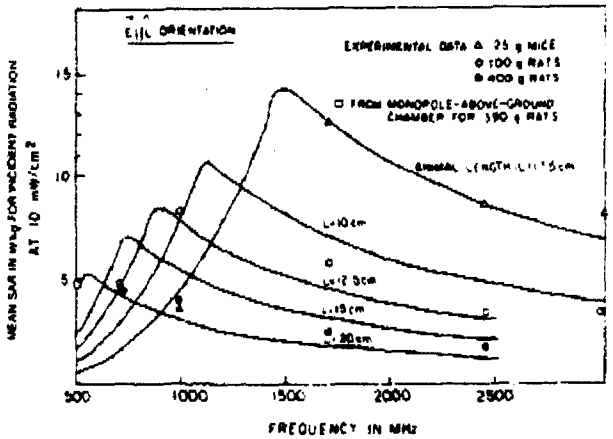

Fig. 3. Theoretical projections (continuous lines) of whole-body SARs of mice and rats of varying mass and axial length for microwave irradiation in the free field. Data points are based on experiments in the free field, or on irradiation in the monopole-above-ground chamber.

results to those of free-space radiation, peak absorption occurs at a frequency about one-half the value for the ungrounded condition. The new resonant frequency is projected to be (31-34) × 1.75/L_m MHz. At resonance, the SAR is about twice that of irradiation in free space.

5. ENERGY DEPOSITION IN THE PRESENCE OF FLAT REFLECTORS

Judging from the success of antenna theory in predicting resonant frequencies and absorption cross sections of different bodies under grounded and ungrounded conditions, highly enhanced SARs are expected for resonant bodies near flat (180°) reflectors and near 90° and other corner reflectors [*Jasik*, 1961]. Gains or enhancements of absorption that are associated with half-wavelength dipoles in the presence of a typically encountered corner reflector are given in Figure 5. To test the validity of antenna theory in predicting enhancements of rates of energy absorption, experiments were performed with a near-resonant (L/λ = 0.417) figurine placed at different distances in front of a flat reflector of dimensions 2.5 λ × 2.5 λ. The enhancement factors relative to the free-space value and corresponding SARs are plotted in Figure 6. Also plotted in the figure are the values of E^2 that would be expected for a standing wave if the target were absent. By comparing Figures 5 and 6, one may note that the degree of enhancement of the SAR is given more accurately by antenna theory than by standing-wave theory. As predicted by antenna theory (Figure 5), a higher SAR is observed for d = 0.125 λ than for 0.25 λ because of coupling of the target to its image. Also, a maximum gain of 4.7 was observed experimentally. This value is in excellent agreement with antenna theory and is 17% higher than the value of 4.0 predicted on the basis of standing-wave theory.

Additional points to note in Figure 6 are: (a) Non-zero energy deposition at d = 0.5 λ, which may be ascribed to absorption due to magnetic fields at this setting, and (b) An enhancement factor of less than 4 at d = 0.75 λ, which may be due to insufficiency of the reflector's dimensions. From antenna theory, a reflector with a width larger than 4 d (in the H plane) is recommended to simulate an infinite plane.

The important features of the above results have been confirmed by experiments that were performed with 100-g Wistar rats; the rats were placed at different locations in front of the flat reflector and were subjected to incident fields at their resonance frequency of 98 MHz. The details and the results of these experiments will be given elsewhere [*Gandhi and Hunt*, 1977].

The enhancement factor as a function of L/λ was measured (Figure 7) with different sizes of figurines at 987 and 2450 MHz. Because of the fairly broad lateral

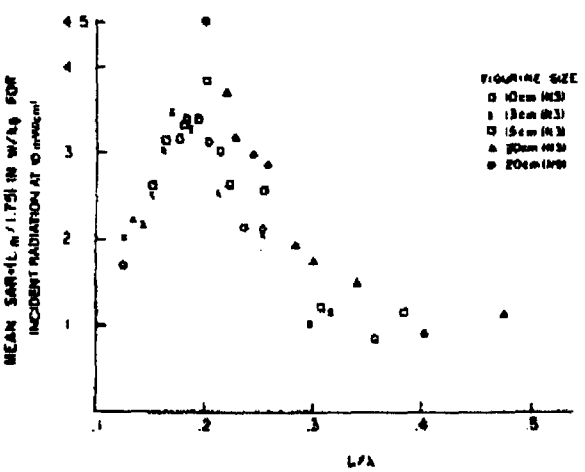

Fig. 4. Projected SARs for a human being of height L (in meters) as a function of L/λ. Feet are in conductive contact with ground. Sample size (N) is shown in parentheses in body of figure.

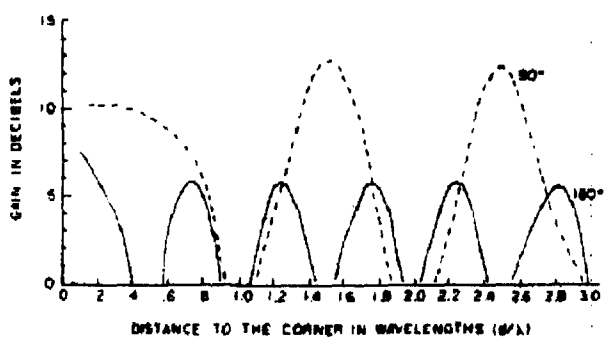

Fig. 5. Gain in rate of energy received by a half-wavelength antenna located at various distances from 90°-corner and 180°-flat reflectors.

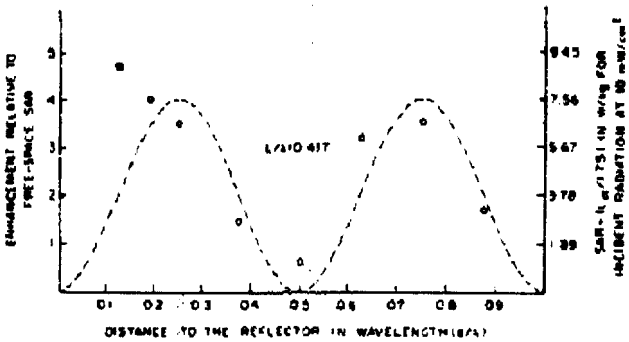

Fig. 6. The data points are measured values of whole-body averaged SARs of a model of a human being of height L (in meters) that is exposed near a flat reflector. The values of E^2 in the absence of the target are shown by the dashed line.

dimensions of the larger targets, a complete set of data was possible only for $d = 3\ \lambda/4$. The points to note in Figure 7 are: (a) The enhancement in SAR at frequencies above resonance diminishes and asymptotically approaches a value of about 2, (b) At frequencies below resonance, a higher gain in SARs from the corresponding free space values (Figure 1) is observed, and (c) For $d = 0.125\ \lambda$, a reduced enhancement factor is observed for smaller targets, which is reminiscent of the standing-wave point of view.

6. ENHANCED ABSORPTION CAUSED BY 90° CORNERS OF REFLECTING SURFACES

Using the near-resonant ($L/\lambda = 0.417$) saline-filled figurine, energy deposition rates were measured at different locations along the diagonal of the 90° corner of several reflectors, each of dimensions $3.5\ \lambda \times 2\ \lambda$ (in the E direction). The measured enhancement factors relative to the free-space value and the corresponding SARs for *man* are plotted in Figure 8. Also shown for comparison in the same figure are the values of E^2 as calculated from standing-wave theory (the kind of values that will be registered by a so-called power-density meter that is calibrated for free-space measurements). As with the flat reflector, the results here also conform to predictions based on antenna theory (Figure 5). Enhancement factors as large as 27 are observed for $d/\lambda = 1.5$. Another point of agreement with antenna theory is a plateau in the enhancement factor at a value of approximately 10.5 for $d/\lambda \leq 0.45$. Reduced gains of hot spots that are closer to the corner compared to $d = 1.5\ \lambda$ are predicted from antenna theory [*Jasik*, 1961] because of mutual-impedance effects.

A measured enhancement factor of 27 (Figure 8) in the SAR is considerably larger than the value of 16 that is predicted by standing-wave theory and is even higher than the value of 20 that is given by antenna theory for a 90° corner of a semi-infinite reflector. Gains higher than those for semi-infinite reflectors have previously been observed [*Cottony and Wilson*, 1958] for corner-reflector antennas of appropriate combinations of width and length. It turns out that our reflector's dimensions of $3.5\ \lambda \times 2\ \lambda$ are, fortuitously, the result of one of the super-gain combinations. There are many other combinations of width and length [*Cottony and Wilson*, 1958] that may also result in high SARs.

To confirm predictions of highly enhanced SARs, experiments were performed with male Wistar rats (104 ± 8.3 g) that were placed $0.44\ \lambda$ and $1.5\ \lambda$ from the corner of the reflectors. The $d = 0.44\ \lambda$ location was the minimum distance to the corner possible with the relatively microwave-transparent rat holder (Figure 9) that we used in our experiments. Also for the $d = 0.44\ \lambda$ experiments, 90° corner reflectors, each of dimensions $3\ \lambda \times 2\ \lambda$ (rather than $3.5\ \lambda \times 2\ \lambda$), were used. From antenna theory, reflectors of dimensions $2\ d$ ($\sim 0.88\ \lambda$)

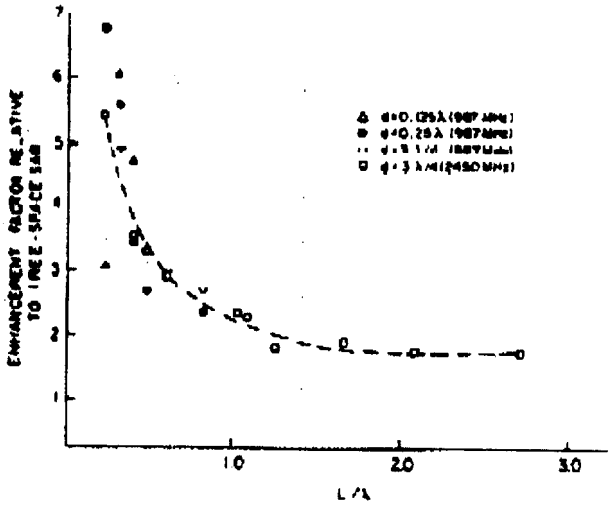

Fig. 7. Enhanced SARs of a body near a flat reflector as a function of the body's length in relation to wavelength of incident radiation.

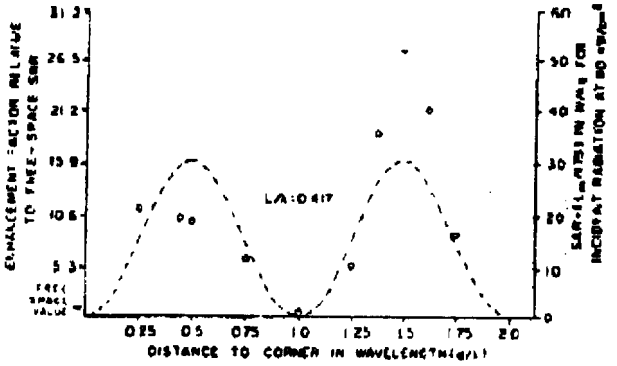

Fig. 8. Whole-body averaged SARs of a model of a human being near a 90°-corner reflector. The dashed line gives values of E^2 in the absence of the model.

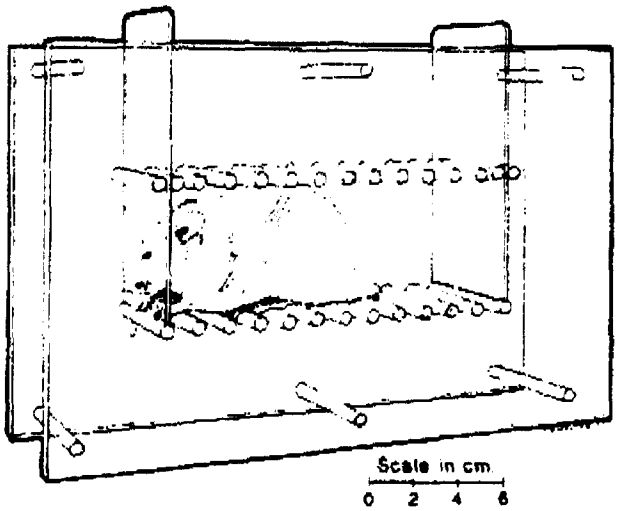

Fig. 9. Semischematic drawing of polycarbonate chamber that was used in irradiation of young rats.

X 0.6 λ would be quite adequate to simulate the semi-infinite sheets that would ideally be needed for 90° corners.

The mean times-to-convulsion together with the standard deviations for four animals for power densities of 3 to 20 mW/cm² are shown in Figure 10. For $d = 0.44\ \lambda$, the mean time-to-convulsion of 225 seconds (for ~ 100-g animals) during irradiation at 15 mW/cm² corresponds to the average of 260 seconds that was observed by *Schrot and Hawkins* [1975] for free-space irradiation at 150 mW/cm². It is apparent, therefore, that the presence of a 90°-corner reflector causes an enhancement in the SAR by a factor of almost 11 as predicted from antenna theory [*Jasik*, 1961]. The relative enhancements at the two locations may be compared by noting that, at power densities of 4.5 and 6 mW/cm² for $d = 1.5\ \lambda$, times-to-convulsion correspond, respectively, to 9.85 and 13.02 mW/cm² for $d = 0.44\ \lambda$. For a target-to-corner separation distance, d, of 1.5 λ, a deposition rate larger by a factor of 2.18 as compared with $d = 0.44\ \lambda$ is consequently obtained from lethality experiments. This result is amazingly close to the relative enhancement of 2.15 observed between the two locations with man-shaped dolls (Figure 8).

The enhancement factors measured for different values of L/λ for a 90°-corner reflector are shown for $d/\lambda = 0.44$, 1.5, and 2.5 in Figure 11. As with a flat reflector, the enhancement in SAR at supraresonant frequencies diminishes and asymptotically approaches a value, in this case, of about 8. Also, for closer spacing to the corner, a reduction in the enhancement factor occurs for smaller values of L/λ. An asymptotic value of 9 would be projected from the simple-minded argument that for targets large compared to a wavelength, a three-sided rather than the four-sided exposure is more realistic. The wave that, for smaller targets, would bounce off the corner is largely masked for large values of L/λ.

From the point of view of standing-wave theory, the fields at different locations in the vicinity of a 90°-corner reflector can be written (see Figure 12) as:

$$\mathbf{E} = \mathbf{E}_1 + \mathbf{E}_2 + \mathbf{E}_3 + \mathbf{E}_4 = \mathcal{E}_{inc}\,\hat{\mathbf{E}} \cdot \{1 + e^{-2jkd} - 2e^{-jkd}\cos ky\} \tag{5}$$

where $k = 2\pi/\lambda$. Peaks of the E field are consequently anticipated not only for axial locations but also for several spots elsewhere (some of which are shown in Figure 12) in the region in front of the reflecting corner.

In order to verify the existence of hot spots elsewhere in the region of a 90°-corner reflector, whole-body

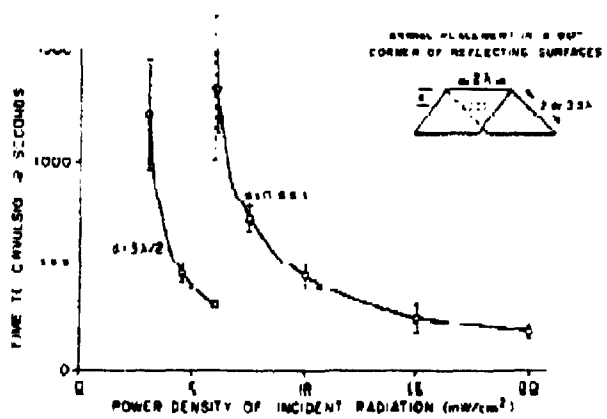

Fig. 10. Cumulative latencies (± SD) of rats (averaged mass near 100 g) as a function of measured power density of incident 987-MHz radiation for two distances of the animal from the corner of the reflector. [illegible]

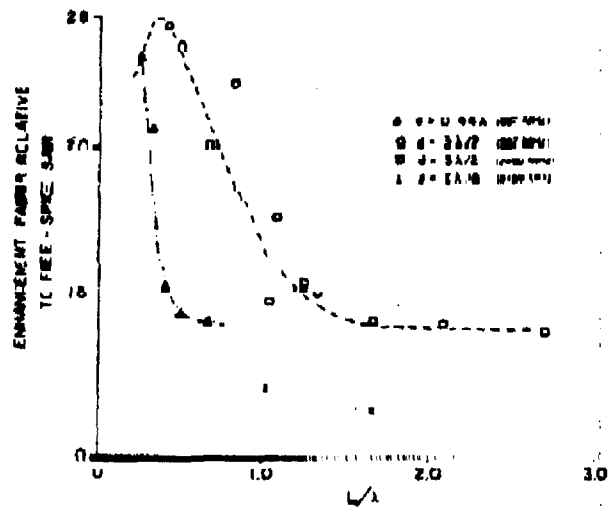

Fig. 11. Enhancement of SARs at a body near a 90° corner reflector.

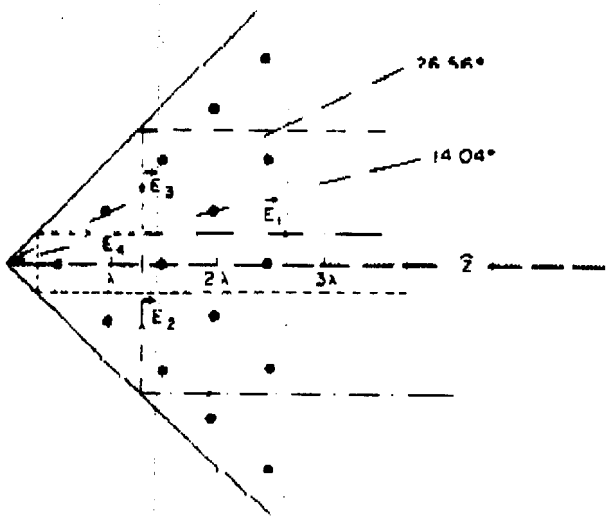

Fig. 12. E-field maxima near a 90°-corner reflector. Filled circles denote areas where a biological body will absorb maximal quantities of energy.

SARs were measured (see Figure 13) at $d/\lambda = 1.0$ with and without the 26.5° tilt of the reflectors around the $\hat{E}$ axis. The "cold" region without the tilt becomes a fairly "hot" region upon tilting. Another implication of this result is that regions associated with high rates of energy deposition are also strongly dependent on directionality of the incident field.

In view of these observations and also since the hot spots may shift rather readily upon placement of other targets in close proximity, the entire region may be considered as one that is potentially capable of creating large field enhancements.

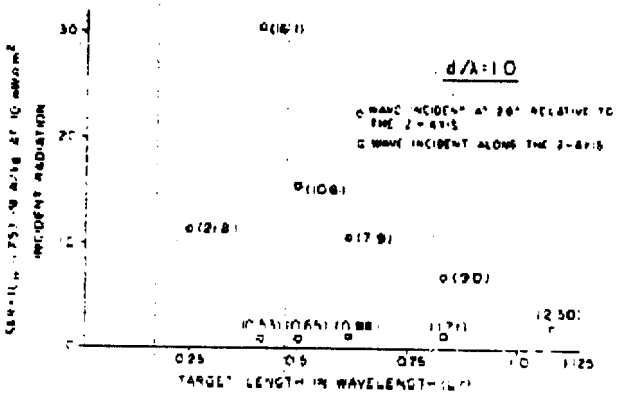

Fig. 13. Whole-body averaged SARs of models of human beings for an $\vec{E} \| \hat{L}$ [illegible] reflectors. Numerical values in parentheses are enhancement factors relative to the free-field SAR.

Both for flat and for 90°-corner reflectors, targets placed in $\mathbf{k} \| \hat{L}$ and in $\mathbf{H} \| \hat{L}$ orientations gave SARs that were considerably enhanced as compared with their respective free-space values. In general, SAR enhancements commensurate with target-averaged E values were measured for L/λ on the order of 0.5 or less. For larger L/λ, enhancements lower than those predicted from a simple-minded E-averaged basis were measured and these are ascribed to significant perturbation of the fields by the targets.

7. CONDITIONS OF HIGHEST RATES OF ENERGY DEPOSITION IN MAN AND ANIMALS

As discussed above, some of the highest SARs in models of man and animals are observed for frequencies close to the region of resonance. Fairly strong enhancements are possible at higher frequencies in the presence of reflecting surfaces, but the enhancement of SARs here is considerably less than that which occurs at resonant frequencies. Enhancement factors just as large or somewhat larger are observed for frequencies below resonance, but the net SARs here, too, are not as large because of the rapid drop-off (see Figure 1) in the SAR on the low frequency side of the resonant curve.

In order to appreciate fully the reflector-caused enhancements of SARs, it should be mentioned that reflectors with dimensions $2\,d \times 1.2\,L$ (in the E direction) are considered adequate to simulate infinite planes. Furthermore, the reflecting surfaces need neither be good conductors nor solid in construction to cause enhancements. Indeed, surfaces of insulating material with conducting rods (oriented along E fields) that are spaced $< 0.1\ \lambda$ act quite effectively as solid conducting surfaces [*Jasik*, 1961].

Whole-body rates of energy absorption for models of man and for animals subjected to 10 mW/cm² incident fields have been calculated for various exposure conditions and are tabulated in Table 1. The rates of energy deposition at resonant frequencies in the presence of a ground plane or a reflector markedly increase and, with grounding and reflection in combination they are truly staggering.

8. CONCLUSIONS

Generalized curves have been given for whole-body absorption of electromagnetic energy by models of human beings as a function of frequency for free space, for electrical contact with ground, and for the presence of reflecting surfaces. Based on these curves, generalized graphs for specific absorption rates for rats and mice are drawn and the results are shown to be in good agreement with experimental data. Tremendous enhancements in rates of energy deposition result for targets that are placed in proximity to reflecting surfaces. Energy deposition rates are given for models of [illegible] density of 10 mW/cm² under various conditions of exposure. SAR values as high as 35 to 70 times the BMR are predicted for adult human beings at resonant fre-

TABLE 1. Rate of whole-body energy absorption in watts by man and animals at 10 mW/cm^2.

70 kg Man (1.75 m Height)	100 g Rat (11.5 cm Length)	400 g Rat (18.9 cm Length)
38 Watts (no reflectance) 0.54 W/kg	_____	_____
19 Watts (50% reflectance) 0.27 W/kg	_____	_____
I. At resonance for free space.		
151 Watts 2.16 W/kg f ≈ 62-68 MHz	0.8 Watts 8 W/kg f ≈ 987 MHz	2 Watts 5 W/kg f ≈ 600 MHz
II. At resonance for conditions of electrical contact with the ground plane.		
2 × 151 = 302 Watts 4.31 W/kg f ≈ 31-34 MHz	_____ _____	_____ _____
III. At resonance for placement in front of a flat reflector		
4.7 × 151 = 710 Watts 10.14 W/kg f ≈ 62-68 MHz	3.8 Watts 38 W/kg f ≈ 987 MHz	9.4 Watts 23.5 W/kg f ≈ 600 MHz
IV. At resonance for placement in a 90° corner reflector.		
27 × 151 = 4077 Watts 58.24 W/kg f ≈ 62-68 MHz	21.6 Watts 216 W/kg f ≈ 987 MHz	54 Watts 135 W/kg f ≈ 600 MHz
V. At resonance in electrical contact with ground plane, in front of a flat reflector.		
2 × 710 = 1420 Watts 20.28 W/kg f ≈ 31-34 MHz	_____ _____	_____ _____
VI. At resonance in electrical contact with ground plane, in a 90° corner reflector		
2 × 4077 = 8154 Watts 116.48 W/kg f ≈ 31-34 MHz	_____ _____	_____ _____

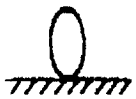

d ≈ 0.125 λ

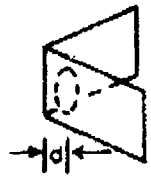

d = 1.5 λ

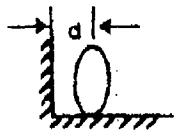

d = 0.125 λ

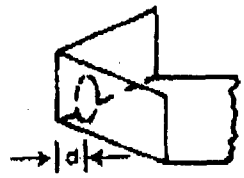

d = 1.5 λ

quencies. The times-to-convulsion of ~ 100-g rats for incident waves of power densities of 3 to 20 mW/cm^2 confirm some of the predictions of enhanced absorption in the presence of reflecting surfaces.

Acknowledgment. This work was supported by U. S. Army Medical Research and Development Command, Washington, D. C., under contract DAMD 17-74-C-4092.

The animals involved in this study were procured, maintained, and used in accordance with the Animal Welfare Act of 1970 and the "Guide for the Care and Use of Laboratory Animals" prepared by the Institute of Laboratory Animal Resources, National Research Council.

REFERENCES

Cottony, H. V., and A. C. Wilson, (1958). gains of finite-size corner reflector antennas. *IRE Trans. Ant. Prop. AP-6*, 366-369.

Dreyfuss, H. (1967). *The Measure of Man, Human Factors in Design*, Whitney Library of Design, New York.

Gandhi, O. P. (1974). Polarization and frequency effects on whole animal absorption of RF energy. *Proc. IEEE*, 62, 1166-1168.

Gandhi, O. P. (1973). Conditions of strongest electromagnetic power deposition in man and animals. *IEEE Trans. Microwave Theory Tech. MTT-22*, 1071-1079.

Exhibit #9

Focus on how much RF is present in a building - due in part to reflections in the building and wire circuits

#9A - Smith, 1978 - shows attenuation drops to zero as frequency increases to 500 MHz.

#9B - Wells, 1976, OT Report 76-98

#9C- Allen et al. 1994, shows 30% of measurements have exposure greater inside than outside if the room is an outside room facing transmitter.

#9D. Taylor et al. shows wiring in house can act as an antenna. Need to consider this when estimating exposure, especially when use telephone.

E 9A

incident plane-wave field. Here, we have assumed $\mu = \mu_0$, $\epsilon = \epsilon_0$ and $\sigma = 0$. Readers may refer to [9] for more numerical data connected with the coupling between infinite cable and the narrow, finite slot.

IV. CONCLUDING REMARKS

For the problem of an infinite cable placed behind a narrow-slot perforated conducting screen, we have obtained an integro-differential equation in an uncoupled, but in a modified form to determine the unknown electric field in the slot. Also, an expression has been given for the current induced on the infinite cable in terms of the slot magnetic-current distribution and the transfer-admittance function. In this approach, the complete coupling between the slot and infinite cable was taken into account. Only the usual thin-wire and narrow-slot approximations were introduced.

One could extend the formulation to a more-general rectangular aperture, but then we would encounter a set of coupled integro-differential equations with semi-infinite integral-kernels, for the field distribution in the aperture. This would be a worthwhile task for the future.

REFERENCES

[1] C. M. Butler and K. R. Umashankar, "Electromagnetic excitation of a wire through an aperture perforated conducting screen," *IEEE Trans. Antennas Propagat.*, vol. AP-24, pp. 456–462, July 1976.

[2] C. M. Butler and K. R. Umashankar, "Electromagnetic penetration through an aperture in an infinite planar screen separating two half spaces of different electromagnetic properties," *Radio Sci.*, vol. 11, no. 7, pp. 611–619, 1976.

[3] K. R. Umashankar and C. M. Butler, "A numerical solution procedure for small aperture integral equations," *EMP Interaction Notes*, Air Force Weapons Lab., Kirtland AFB, NM, July 1974.

[4] D. A. Hill and J. R. Wait, "Coupling between a dipole antenna and an infinite cable over an ideal ground plane," *Radio Sci.*, vol. 12, no. 2, pp. 231–238, Mar./Apr. 1977.

[5] J. R. Wait, *Electromagnetic Waves in Stratified Media*, 2nd ed., New York: Pergamon Press, 1970.

[6] M. Abramowitz and I. Stegun, *Handbook of Mathematical Functions*, New York: Dover, 1965.

[7] J. R. Wait, *Electromagnetic Radiation From Cylindrical Structures*. New York: Pergamon Press, 1959.

[8] C. M. Butler, K. R. Umashankar, and C. E. Smith, "Theoretical analysis of the wire biconical antenna," *Tech. Rep.*, U.S. Army Stratcom, Ft. Huachuca, AZ, Jan. 1975.

[9] K. R. Umashankar and J. R. Wait, "Electromagnetic coupling to an infinite cable placed behind a slot perforated screen," EMP Interaction Notes, Note 330, Air Force Weapons Lab., Kirtland AFB, NM, June 1977.

Attenuation of Electric and Magnetic Fields by Buildings

ALBERT A. SMITH, JR., SENIOR MEMBER, IEEE

Abstract—Results of an empirical investigation of the shielding properties of seven buildings, ranging from single-family detached residences to multistory office buildings, are presented. Both electric-field and magnetic-field attenuations were measured in the frequency range of approximately 20 kHz to 500 MHz.

Key Words: Shielding properties, buildings, 20 kHz–500 MHz.

INTRODUCTION

QUANTITATIVE DATA on the attenuation of external electromagnetic fields by building structures is useful in a number of engineering applications. For instance, in the field of EMC, building attenuation data can be used to predict the susceptibility of electronic systems to high-level lightning, broadcast and radar fields, and to develop radiated-susceptibility limits [1]. Communication and broadcast engineers, concerned with the reception of radio paging signals and AM, FM, and TV broadcast fields inside buildings, must account for building attenuation when making path-loss analyses [2]. With regard to susceptibility, the inherent shielding provided by building structures is desirable, while for radio communications it is a decided disadvantage.

Mir and White [1] measured the attenuation of electric fields by steel-frame multistory office buildings in the frequency range of 500 kHz to 500 MHz. Other investigators measured the attenuation of buildings at two or three frequencies [2]–[5]. Earlier studies on the insertion loss of walls are reported in [6] and [7].

Manuscript received June 20, 1977; revised February 27, 1978.

The author is with the Electromagnetic Compatibility Laboratory, System Communications Division, IBM Corporation, Kingston, NY 12401. (914) 383-2364.

0018-9375/78/0800-0411$00.75 © 1978 IEEE

This paper presents the results of an empirical investigation of the shielding properties of seven buildings, ranging from single-family detached residences to multistory office buildings. Both electric-field and magnetic-field attenuations were measured in the frequency range of about 20 kHz to 500 MHz.

MEASUREMENTS

A brief description of the seven buildings measured is given in Table I. Photographs of their exteriors are above the attenuation curves (Figs. 1-14). The buildings were selected to provide as wide a range of building attenuations as possible within the constraints imposed by the limited sample size, building availability, and the ground rule that the samples had to be reasonably representative of the types of buildings in which electronic equipment, office machines, or data-processing systems are commonly found.

The *a priori* assumption was that a building's attenuation could be correlated with the amount of metal in the building. Thus Buildings 1-7 have progressively increasing amounts of metal.

The general approach was to measure the electric and magnetic field strength of existing ambient broadcast signals, both outside and inside a building, defining building attenuation as the ratio of the external fields to the fields inside, expressed in decibels.

In the geographical area where the measurements were made (Ulster, Green, Dutchess, and Albany counties of New York State), there were no stable ambient signals in the spectrum between the AM broadcast band and the FM band. To fill this gap, a mobile transmitter, operating at 7, 21, and 29 MHz, at distances ranging from 500 m to 2000 m, was used as the source.

A number of high-level VLF and LF signals were detectable (notably NSS at 18 kHz and WGU20 at 180 kHz). Thus it was possible to obtain building attenuation data well below the AM broadcast band (an advantage not enjoyed by Mir and White [1], who made measurements in Bethesda, MD, and Montreal, Ottawa, and Toronto, Canada).

Outside fields were measured at ground level at a number of locations around the peripheries of Buildings 1-4. The measurements were taken at considerable distances from the buildings since the outside fields in close proximity to the walls (e.g., within 3 m) exhibited attenuations of the same order as the fields inside.

At Buildings 6 and 7, external fields were measured on the roof since there was insufficient open space at ground level. Outside fields at Building 5 were measured at both ground level and on the roof. (The measured data showed that the field strength on the roof differed little from the ground-level field strength, even at VHF and UHF frequencies. That is, because of the conducting surface of the roof, there was no field height-gain.) The external reference field strength at each frequency was defined as the mean value of the outside measurements.

The number of locations at which interior measurements were made depended on the size of the buildings and varied from a single location in Building 1, to 12 locations in Building 7. The total number of interior measurements exceeded 8000.

Below 7 MHz, the vertical component of the electric field was measured, while above 7 MHz both vertical and horizontal electric-field components were measured. Generally [illegible] horizontal component of the magnetic field was [illegible]. The receiving antennas were rotated in azimuth for [illegible] signal strength when measuring the horizontal field [illegible]ents.

From 20 to 80 kHz, the Electro-Metrics EMC-25 was used. Schwarzbeck FSME 1515 and VUME 1520A field-strength meters were employed from 80 kHz to 500 MHz. Receiving antennas for electric-field measurements were: the Electro-Metrics RVR-25 monopole below 7 MHz, and the Singer MD-105-T1 broad-band dipole above 7 MHz. Magnetic-field measurements were made with Singer loops LG-105A, LP-3-105, and LP-105.

TABLE I
DESCRIPTION OF BUILDINGS

Building No.	Classification	Description
1	Single-family detached residence	Split level ranch, wood framed, with wood and brick siding, aluminum foil covered insulation in the ceiling, and an 18 inch steel I-beam under the floor to support the floor joist.
2	Single-family detached residence	Wood-framed raised ranch with aluminum siding covering the upper level and concrete block walls on the lower level. There is a brick veneer trim on the main level.
3	Single-story concrete block	Concrete block building with a large metal-frame store-front window across the front. The structure is frame with steel columns and a steel bar joist supported roof, and is constructed on a standard reinforced concrete slab on grade. The interior is divided into cubicles with lightweight steel and glass partitions and a suspended ceiling with recessed fluorescent lighting fixtures. An extensive array of ducts, pipes and cable occupies the space above the suspended ceiling.
4	Single-story concrete block	Concrete block steel frame building constructed on a reinforced concrete slab on grade. There are insulated steel frame windows and doors in the walls. The interior area [illegible] similar to that of Building No. [illegible]
5	Multistory office	Four-story steel frame [illegible] with prestressed concrete [illegible] panels and continuous [illegible] windows on three sides. The [illegible] side is covered with [illegible] wall panels and has a [illegible] aluminum vertical window [illegible] roof in the center of the [illegible] floors are corrugated [illegible] with poured concrete. The [illegible] description is similar to that of Building No. 3.
6	Multistory office	Four-story steel frame [illegible] with brick exterior [illegible] steel floors covered with [illegible] crete, and isolated aluminum [illegible] windows. The interior [illegible] is similar to that of [illegible]
[illegible]	Multistory office	Twenty-story steel frame [illegible] building with marble [illegible] panels and continuous [illegible] windows on all four sides. [illegible] steel columns are placed [illegible] the floors. The floor [illegible] steel covered with poured [illegible] The interior is partitioned [illegible] There are few interior [illegible] and partitions, and [illegible] structure is non-conducting [illegible] There is a suspended [illegible] recessed fluorescent [illegible] on each floor. Electrical [illegible] is routed in raceways [illegible] and all outlets on the [illegible] flush with the corridor [illegible] wall.

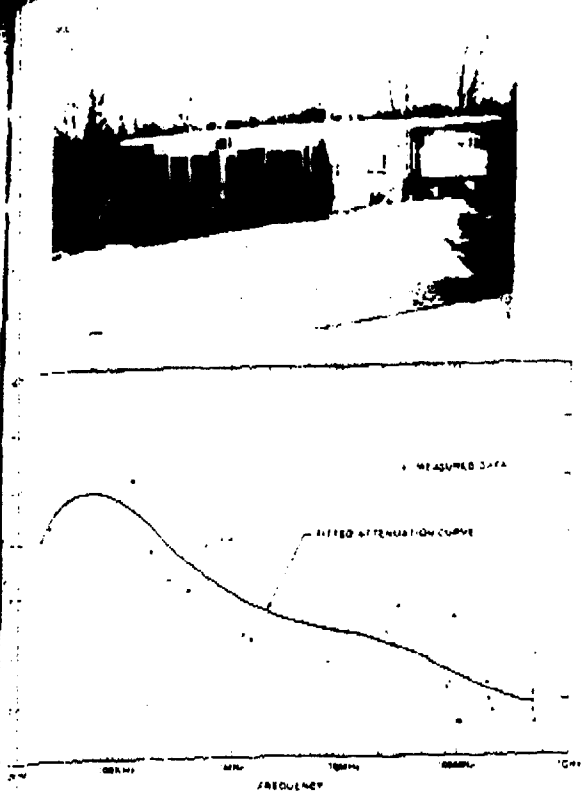

Fig. 1. Electric-field attenuation, single-family residence with wood and brick siding (Building No. 1).

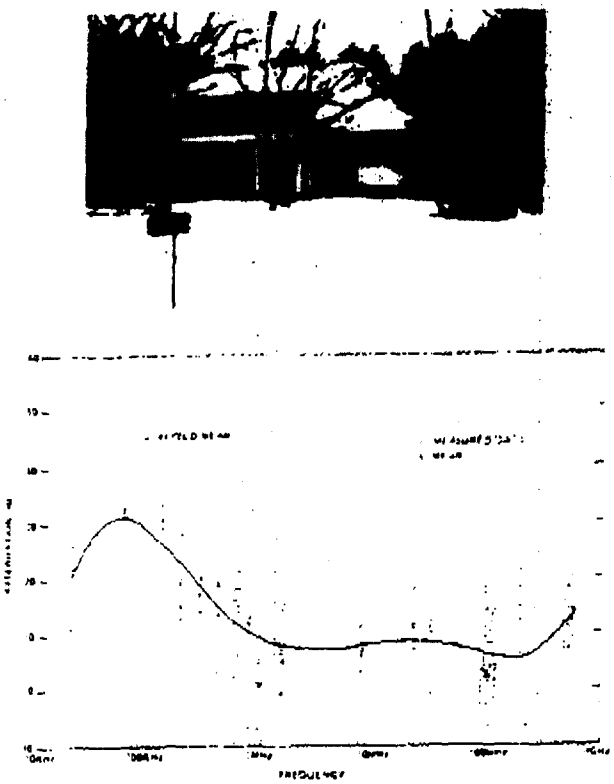

Fig. 3. Electric-field attenuation, single-family residence with aluminum siding (Building No. 2).

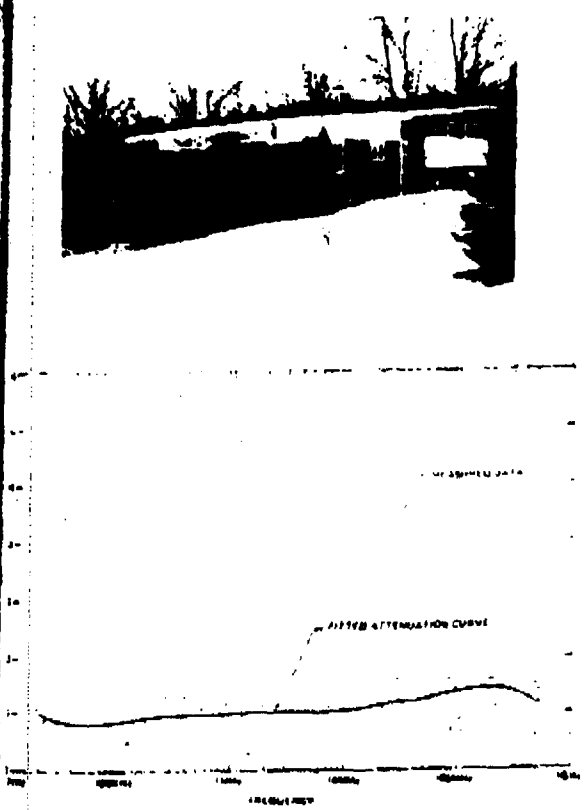

Fig. 2. Magnetic-field attenuation, single-family residence with wood and brick siding (Building No. 1).

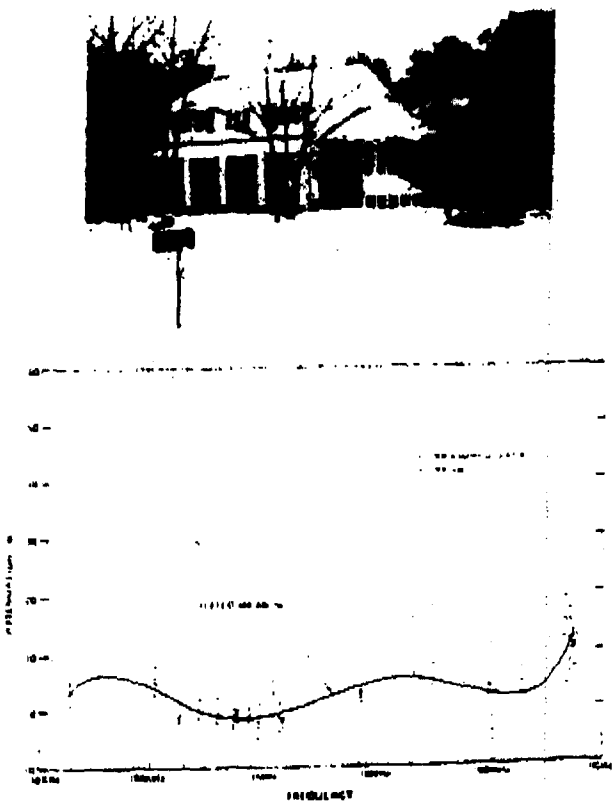

Fig. 4. Magnetic-field attenuation, single-family residence with aluminum siding (Building No. 2).

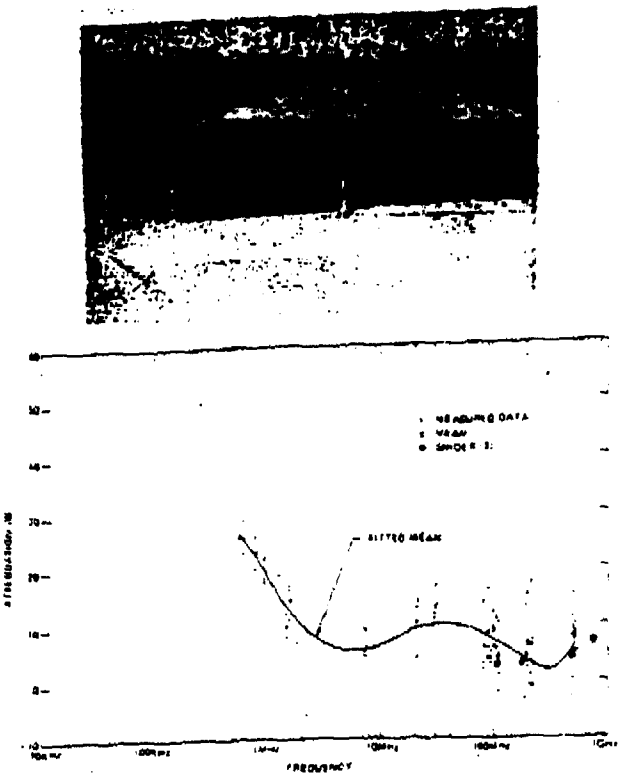

Fig. 5. Electric-field attenuation, single-story concrete-block building (Building No. 3).

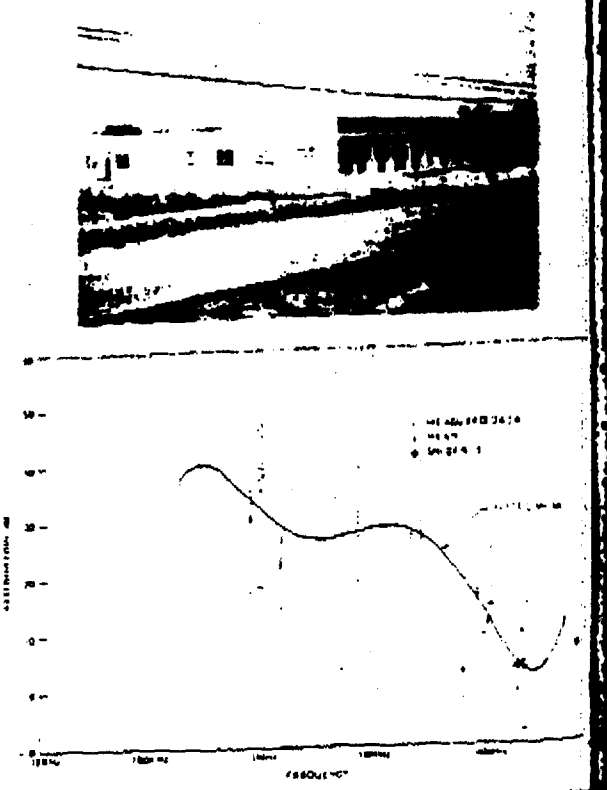

Fig. 7. Electric-field attenuation, single-story concrete-block building (Building No. 4).

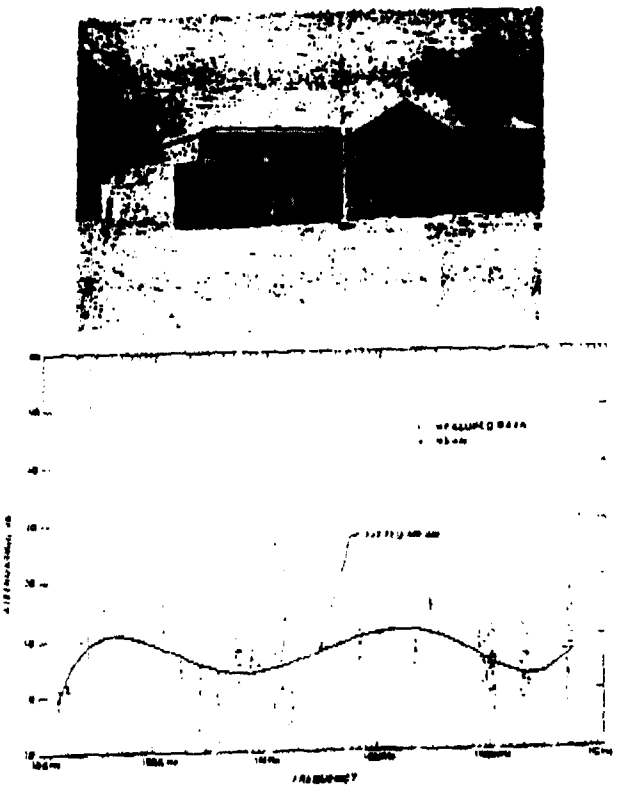

Fig. 6. Magnetic-field attenuation, single-story concrete-block building (Building No. 3).

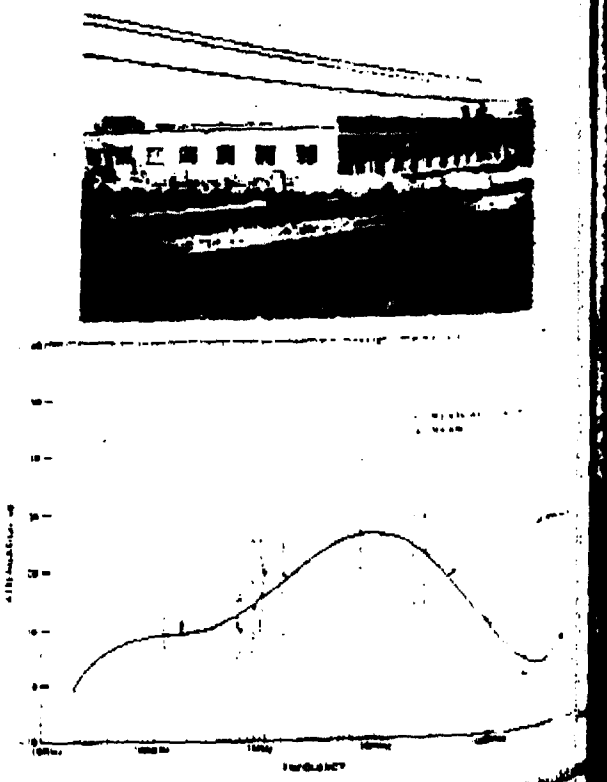

Fig. 8. Magnetic-field attenuation, single-story concrete-block building (Building No. 4).